SECTION I

RESEARCH IN PROGRESS

Comparison of $^{24,25,26}Mg(p,n)^{24,25,26}Al$ Cross Sections with Giant M1 Strength

U.E.P. Berg, Sam M. Austin, R. DeVito, A.I. Galonsky and W.A. Sterrenburg

While substantial M1 strength has been found in the light nuclei, much less is known about its location for A>40. In these heavier nuclei the transition strength appears to be spread over a wide range of excitation and to be fragmented among many levels, strongly reducing the sensitivity of the usual experimental techniques. It is then useful to search for other experimental probes which, while perhaps less precise, are more sensitive or selective. The (p,n) reaction at E_p>30 MeV shows promise in this regard. For example, there is convincing evidence[1] that the $^{90}Zr(p,n)^{90}Nb$ reaction at 45 MeV strongly excites analogs of M1 strength in ^{90}Zr. (p,n) reactions may become a very useful probe, especially in heavier nuclei, of spinflip-isospin flip strength.

For the charge-exchange probe to provide quantitative information one needs to calibrate it at energies where the reaction mechanism is reasonably well understood and for nuclei where individual states can be resolved. Furthermore, detailed electromagnetic information must be available. Our data at 35 MeV for the $^{24,25,26}Mg(p,n)^{24,25,26}Al$ reactions satisfy these conditions.

That one can use charge-exchange reactions to search for M1 strength lies in the similarity of the operator for the two processes. One therefore expects M1 transitions which are strong to be strong in (p,n). Since, e.g., absorption of magnetic dipole radiation leads to strong 1^+, T=1 ($T_3 = \frac{N-Z}{2} = +1$) states near 10 MeV in ^{26}Mg we expect strong (p,n) transitions to their analogs in ^{26}Al with $J = 1^+$, T=1 (T_3=0) at about 10 MeV above the isobaric analog of the ^{26}Mg ground state.

Figure 1 shows the angular distribution of the $^{26}Mg(p,n)$ cross section to an isolated 1^+ state at 1.06 MeV in ^{26}Al. This $\sigma(\theta)$ is used as a standard to identify other 1^+ states. The distorted wave calculations show that the 1.06-MeV state is reasonably well represented by the DWBA approximation and that the shape is stable against changes in excitation energy. We find that five states in ^{26}Al have 1^+ shapes and that they lie near 10 MeV (E_x=9.44, 9.89, 10.47, 10.83 and 11.21 MeV) as expected. The angular distribution of the 9.44 MeV state, for example, which is shown in Fig. 1, is very much like that of the 1.06-MeV state. Also shown is the angular distribution of a known 2^+ state at 3.16 MeV; from this plot and others it is clear that shapes corresponding to 1^+ states are sufficiently distinctive.

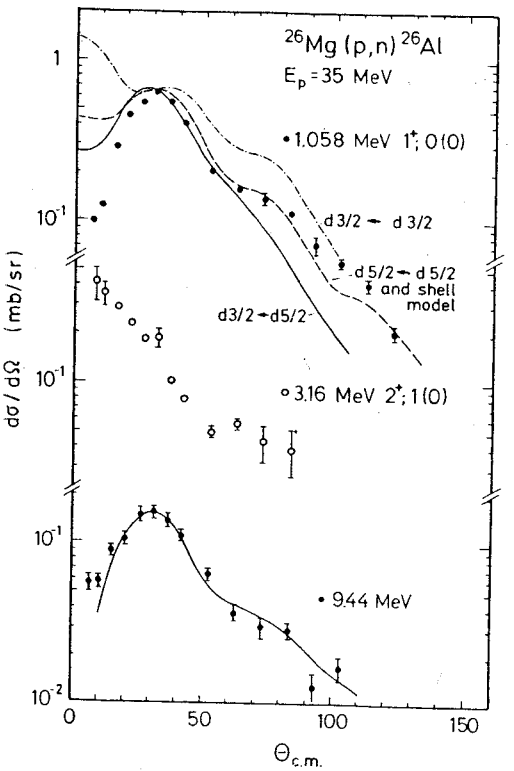

FIG. 1. Angular distributions of the well-resolved 1^+ state at 1.06 MeV, of the 2^+ state at 3.16 MeV, and of the 9.44-MeV representative of the 1^+ states near 10 MeV. The curve at the 9.44-MeV data is a copy of the shape of the 1.06-MeV cross section. Inserted are microscopic DWBA results using particle and shell model[3] transition densities.

The results from our (p,n) measurements are summarized and compared with B(M1) values from inelastic electron scattering[2] in Fig. 2. For $^{24,26}Mg$, where spin assignments are known, Fagg's observations[2] represent over 85% of the sum rule strength.[3] In almost all cases there is a surprisingly good 1:1 agreement subject to an overall normalization factor. The spins of the four high lying states in ^{25}Mg are unknown, and for these the statistical factor $g=(2J_o+1)/(2J+1)$ has been arbitrarily set to one. The total error bars for these states have been hatched, indicating that the three values, g=1.5, 1.0, and 0.75, are possible. Transition strengths of close-lying states, when resolved in the (p,n) experiment but not in (e,e'), have been combined for comparison.

Discrepancies between (e,e') and (p,n) occur for the 11.76-MeV state in ^{25}Mg and the 13.33-MeV state in ^{26}Mg. These states are easily seen in (e,e'), but their analogs are only weakly populated. For the 7.03-MeV state in

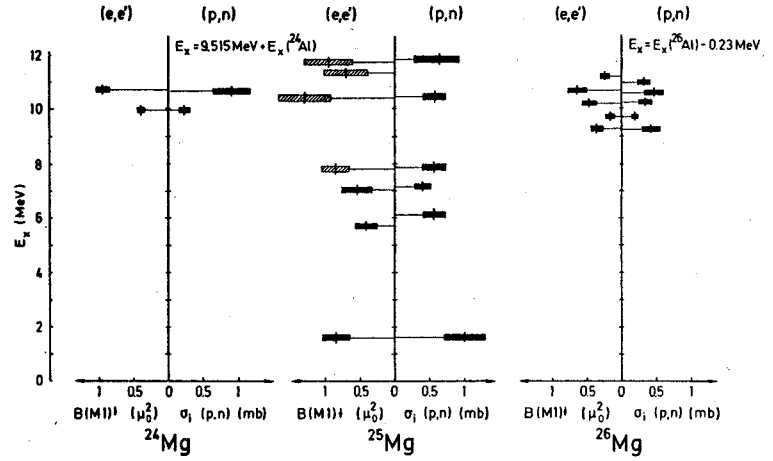

FIG. 2. Comparison of B(M1) strengths from the electromagnetic interaction (Ref. 2) with (p,n) cross sections integrated from 7° to 103°.

^{25}Mg it appears from the raw (e,e') spectra of Ref. 2 that the B(M1) may be overestimated.

The generally close agreement of the (e,e') and (p,n) results is somewhat surprising, since the isoscalar current terms in the M1 operator, while generally of secondary importance, are not always negligible.[4] Indeed, the shell model calculations[3] predict strong current effects, inconsistent with the (e,e') data, for the strong M1 states in ^{26}Mg. The results shown in Fig. 2 can be taken to indicate that current effects are about the same, and presumably small, and the isoscalar part is negligible for those strong M1 states in the Mg isotopes. It is possible that current effects explain the discrepancies noted above.

---

1. R.R. Doering, A. Galonsky, D.W. Patterson, and G.F. Bertsch, Phys. Rev. Lett. 35, 1691 (1975).
2. L.W. Fagg, Rev. Mod. Phys. 47, 638 (1975).
3. B.H. Wildenthal, in "Elementary Modes of Excitation in Nuclei" LXIX Corso, edited by the Soc. Italiana di Fisica, Bologna, Italy (1977) p. 383; and private communication.
4. S.S. Hanna, Photonuclear Reactions I, ed. S. Costa and C. Schaent, (Springer-verlag, Berlin, 1977) p. 275.

^{90,92,94}Zr(p,n)^{90,92,94}Nb at 80, 120 and 160 MeV

W. Sterrenburg, S. Austin, A. Galonsky and T. Nees;[a] D. Bainum;[b] J. Rapaport;[c] E. Sugarbaker;[d] C. Foster;[e] C. Goodman and D. Horen;[f] C. Goulding and M. Greenfield[g]

The IAS and Gamow-Teller resonances have been measured using the beam swinger facility at IUCF with proton energies of 79.2, 119.4, and 160.3 MeV. The targets were ^{90,92,94}Zr of thickness 77.5, 25.4, and 41.6 mg/cm^2, respectively. Two 6" x 6" x 40" NE102 detectors were used with neutron flight paths of 46.5 m for the 80 MeV run and 70.15 m for the 120 MeV and the 160 MeV runs.

Time calibrations were made with (p,n) on a $^{12+13}$C target, and cross sections were normalized to the ^{7}Li(p,n) reaction.[1] The fitting program QUAGMIRE was used to analyze the (p,n) spectra with Gaussian peaks and quadratic backgrounds. Sample spectrum analyses are shown in Figures 1 through 3. Resulting energies and widths for 80 MeV and 120 MeV are given in Table 1. The 160 MeV analysis is in progress.

Angular distributions for ^{90}Zr at 80 MeV and 120 MeV are shown in Figures 4 and 5. The angular distributions for ^{92,94}Zr have the same characteristics as that for ^{90}Zr. The two peaks (11 and 12) lying between 2 and 5 MeV above the IAS are tentatively assigned as being components of the 1^+ giant GT resonance because of the similarity of their distributions with the cluster of 1^+ states lying below the IAS. We note that use of a single Gaussian peak cannot result in good fits to the spectra.

The angular distribution of the state lying betwen 12 and 14 MeV above the IAS implies an L=1 transfer. However, the spin assignment is more complicated due to contributions by both spin-flip and nonspin-flip transfers. A nonspin-flip transfer yields $0^+ \rightarrow 1^-$, while the spin-flip transfer allows $0^+ \rightarrow 0^-, 1^-, 2^-$. The differences in the excitation energies for Peak 21 at 80 MeV and 120 MeV in Table 1 and at lower energies[2] might be understood as due to the growing dominance of the spinflip transfer at higher energies[3] and the fact that the four states for L=1 transfer are not degenerate.[4]

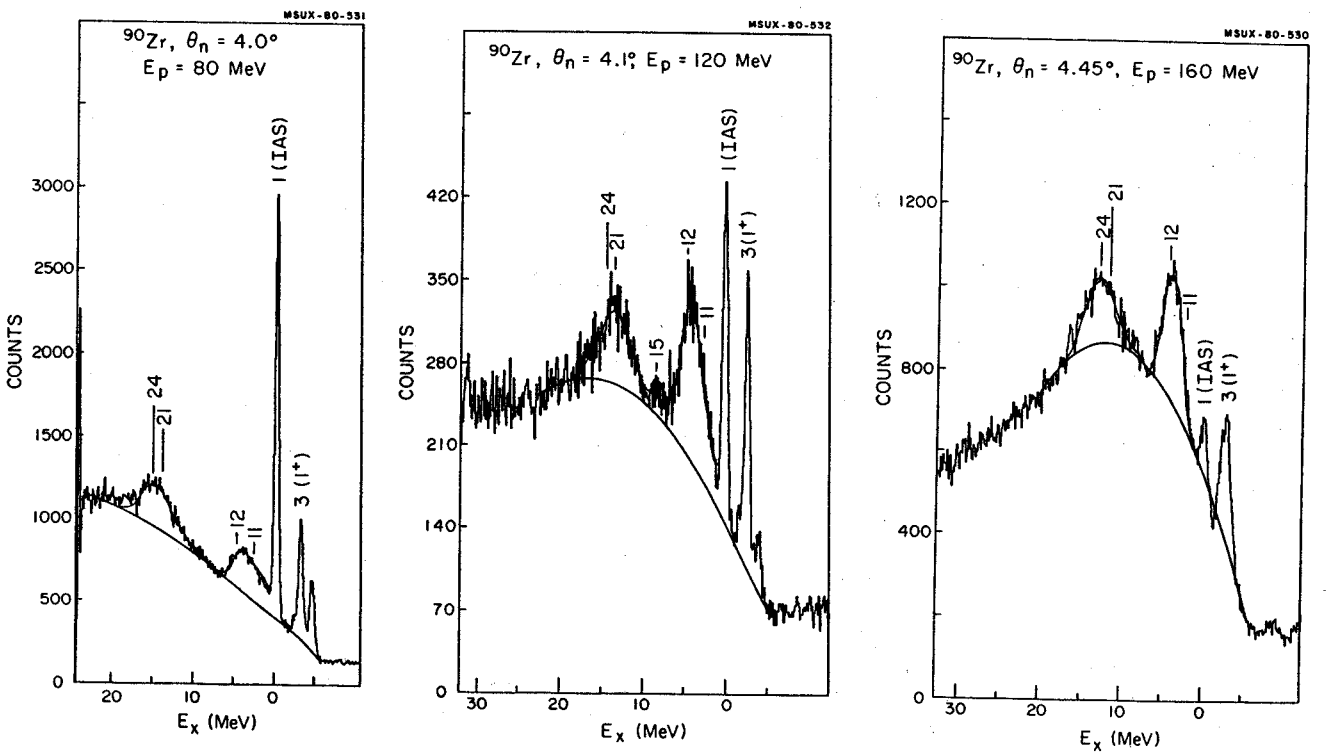

FIG. 1, 2 and 3. Samples of QUAGMIRE fitting of ^{90}Zr (p,n) at $\theta_n \simeq 4°$ for E_p = 80, 120 and 160 MeV. Only the principle peaks are labeled. The analysis of the 160 MeV spectrum is a preliminary fit.

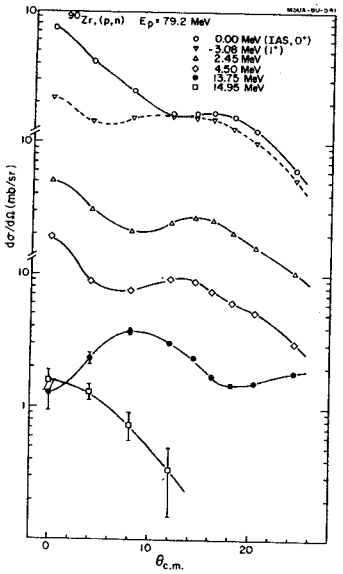

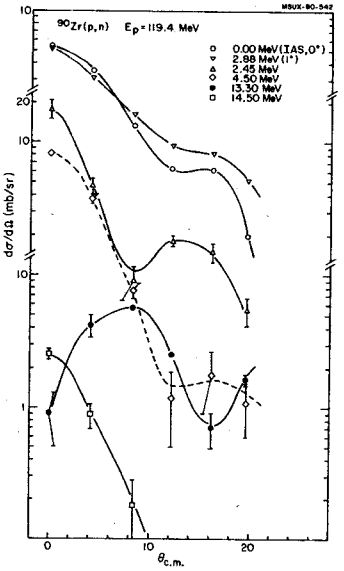

FIGS. 4&5. Angular distributions of the principle peaks given in Table 1 for ^{90}Zr(p,n) at E_p = 80 MeV and 120 MeV. Curves through the data points are not theoretical fits.

Table 1. Excitation energies (above the IAS) and widths of the principal peaks seen in ^{90,92,94}Zr(p,n) ^{90,92,94}Nb at E_p = 80 MeV and 120 MeV. Note the different excitation energies of Peaks 21 and 24 at 80 MeV and 120 MeV for all three targets.

	PEAK	E_p = 80 MeV		E_p = 120 MeV	
		E±ΔE(MeV)	Γ±ΔΓ(MeV)	E±ΔE(MeV)	Γ±ΔΓ(MeV)
^{90}Zr(p,n)^{90}Nb	3 (1^+)	-3.01±0.08	0.72±0.02	-2.90±0.23	0.76±0.04
	1 (IAS)	0.0	0.534±0.017	0.0	0.677±0.041
	11	2.45±0.15	4.1±0.3	2.45±0.15	4.1±0.3
Q(IAS)=-12.00 MeV	12	4.50±0.10	2.0±0.3	4.50±0.10	2.0±0.3
	21	13.75±0.30	4.64±0.32	13.30±0.35	4.64±0.32
	24	14.95±0.30	3.50±0.41	14.50±0.35	3.50±0.41
^{92}Zr(p,n)^{90}Nb	1 (IAS)	0.0	0.415±0.007	0.0	0.580±0.017
	11	2.70±0.20	4.1±0.3	2.70±0.20	4.1±0.3
	12	3.60±0.15	2.0±0.3	3.60±0.15	2.0±0.3
Q(IAS)=-11.812 MeV	21	13.25±0.25	4.64±0.32	12.60±0.30	4.64±0.32
	24	14.75±0.30	3.50±0.41	14.10±0.35	3.50±0.41
^{94}Zr(p,n)^{94}Nb	1 (IAS)	0.0	0.484±0.009	0.0	0.607±0.019
	11	2.10±0.17	4.1±0.3	2.10±0.17	4.1±0.3
	12	3.08±0.15	2.0±0.3	3.08±0.15	2.0±0.3
Q(IAS)= -11.68 MeV	21	12.73±0.37	4.64±0.32	12.00±0.45	4.64±0.32
	24	14.63±0.48	3.50±0.41	13.90±0.52	3.50±0.41

a Michigan State University, East Lansing, MI 48824.
b Emporia State University, Emporia, KS 66801.
c Ohio University, Athens, OH 45701.
d University of Colorado, Boulder, CO 80309.
e Indiana University, Bloomington, IN 47405.
f Oak Ridge National Laboratory, Oak Ridge, TN 37830.
g Florida A & M University, Tallahassee, FL 32307.

1. J. Rapaport, D.E. Bainum, C.D. Goodman, C.C. Foster, T.E. Ward, C.A. Gouling and M.B. Greenfield, IUCF Scientific and Technical Report, p. 27, 1979; and C.A. Goulding, M.B. Greenfield, D.E. Bainum, J. Rapaprot, C.C. Foster, T.E. Ward, C.D. Zafiratos, S.D. Schery, and C.D. Goodman, Nucl. Phys. A331, 29 (1979).
2. W. Sterrenburg, S. Austin, R. Devito, and A. Galonsly, elsewhere in this report, and Phys. Rev. Lett., submitted.
3. W.G. Love, Proc. Conf. (p,n) Reactions and Nucleon-Nucleon Forces, Telluride, March 1979, Plenum, p. 23; F. Petrovich, op. cit., p. 115.
4. F. Krmpotic, K. Ebert and W. Wild, Nucl. Phys. A342, 497 (1980).

Q-Value Systematics for Isovector Giant Resonances Excited by (p,n) Reactions on Zr, Nb, Mo, Sn and Pb Isotopes

W.A. Sterrenburg, Sam M. Austin, R.P. DeVito and Aaron Galonsky

We have used the (p,n) reaction at 45 MeV to systematically study two broad peaks found previously[1,2] with the target ^{90}Zr. Both peaks have now been observed with all but one of 17 targets from ^{90}Zr to ^{208}Pb. Energy systematics favor the conclusion that these peaks are anti-analogs of the giant M1 and E1 resonances in the target nucleus. The relevant states of a target and its isobaric daughter nucleus are illustrated in Fig. 1.

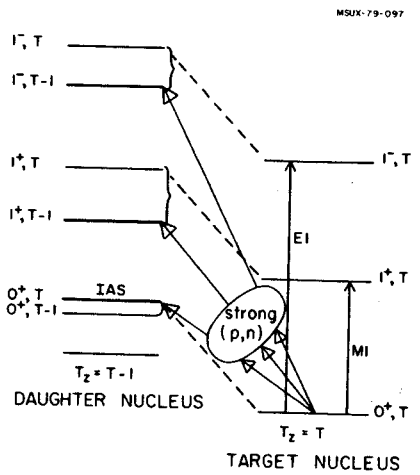

FIG. 1. Some states of the target nucleus (T_z=T) and their analogs (isospin = T) and anti-analogs (isospin = T-1) in the T_z=T-1 nucleus resulting from a (p,n) reaction. The target states are the ground state and the M1 and E1 giant resonant states. Isospin geometry strongly favors the three transitions indicated.

Figure 2 shows neutron time-of-flight spectra for four Sn isotopes. In addition to the IAS at about 31 MeV neutron energy and the sharp γ-ray peak leaking through the pulse shape discriminator, two broad peaks are clearly visible in all four spectra. The smooth curves are fits through the data assuming quadratic backgrounds and Gaussian peaks. The widths for both broad peaks were fixed at 3.6 MeV for all Sn isotopes, and a search was made only for the centroids and the heights. As one can see, both broad peaks shift towards the IAS as the neutron excess increases. This effect is even more visible in Fig. 3 where the neutron spectra are shifted in energy so that the IAS

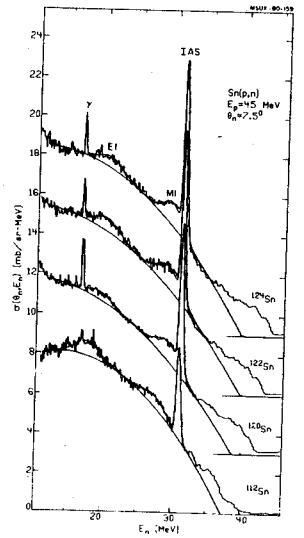

FIG. 2. Neutron spectra for ^{112,120,122,124}Sn (p,n) measured at 7.5°. The baselines for ^{120}Sn, ^{122}Sn and ^{124}Sn are shifted for display purposes. The solid curves are fits to the data assuming quadratic backgrounds and Gaussian peak shpaes.

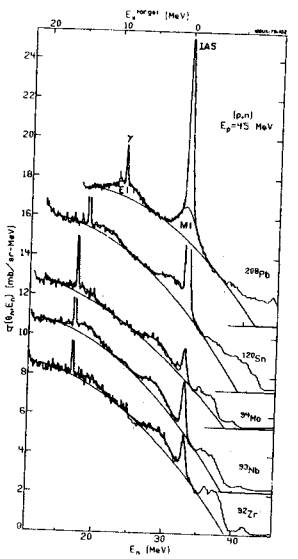

FIG. 3. Neutron spectra for ^{92}Zr, ^{93}Nb, ^{94}Mo, ^{120}Sn, and ^{208}Pb corrected for Coulomb displacement energies. The ^{93}Nb spectrum was measured at 11°, the others at 7.5°. The upper four spectra are shifted for display purposes. The bottom scale gives the neutron energies for ^{92}Zr only; the upper scale gives the calibration for the excitation energies in all the target nuclei.

peaks all fall on the same vertical line, thereby graphically correcting for the Coulomb displacement energies. Hence, points on a vertical line correspond to the same excitation energy (E_x) in every target. For ^{208}Pb the peak at lower E_x lies squarely under the IAS. In this case we show an additional result of the fitting in which the sharp IAS is neglected. Compared to the Sn targets in which the broad peaks had widths of 3.6 MeV, in ^{208}Pb the widths were only 2.9 MeV, whereas in Zr, Nb, and Mo they were slightly larger, 3.8 MeV. As for excitation energies, we conclude that both broad features shift rapidly toward the IAS with increasing (N-Z).

The most natural interpretation of this phenomenon is that the observed peaks are antianalog states (AAS) of excitations in the parent nucleus and that the increased splitting of the analog state (AS) and the AAS with increasing (N-Z) is what is observed. The higher (lower) lying peak is assumed to be the T-1 antianalog of the E1(M1) resonance of isospin T in the parent nucleus. The observed shifts are much larger than the $A^{-1/3}$ shifts that would be associated with AS transitions. That the observed peaks are AAS transitions in also consistent with the relative suppression (by an order of magnitude or more for the nuclei studied) of the AS transitions by geometrical isospin factors associated with the neutron excess.

We now consider these enhancements in more detail beginning with that at higher E_x which we assume is the antianalog of the giant (E1) dipole resonance in the target nucleus. The E_x of the E1 resonance, E_x (target), is well known. The difference between this energy and the E_x (above the IAS) of the broad peak is $\Delta E^- = E(T) - E(T-1)$, the amount of the isospin splitting. Formally, $\Delta E^- = E_x(\text{target}) - [Q(\text{IAS}) - Q(T-1)]$. The splittings ΔE^- are listed in Table I. The uncertainties are principally those of Q(T-1), the quantities measured here.

Several calculations[3,4] have been done for ΔE^+, the isospin splitting between the T+1 and T components of the giant resonance, and some measurements[5,6] have been reported. The results, correlated through a Lane type, or isovector, potential give:

$$\Delta E^+ = (T+1)E_v \text{ with } E_v = V/A \text{ and } V \cong 60 \text{ MeV}.^4 \qquad (1)$$

This model predicts that $\Delta E^- \cong 60\ T/A$; our results are all smaller than this prediction. In a more general treatment[7,8] the isotensor contributions may not be neglected, and one obtains

$$\Delta E^+ = (T+1)[E_v + (2T-1)E_t] \quad \text{and}$$
$$\Delta E^- = T[E_v - (2T+3)E_t] \quad . \qquad (2)$$

Both parameters, E_v and E_t, may be determined for a nucleus in which both ΔE^+ and ΔE^- have been measured. For nuclei having published values of ΔE^+ to use with our ΔE^- measurements

Table I. Measured Q-values for the antianalog states and deduced values for ΔE^-, i.e., for the T, T-1 isospin splittings of the M1 and E1 resonances. All energies are in MeV.

		M1			E1		
Target	-Q(IAS)	-Q(T-1)	E_x(tgt)[a]	E^-	-Q(T-1)	E_x(tgt)	E^-
^{90}Zr	12.00	15.08±0.16	8.93	5.87	26.6±0.3	16.79	2.2±0.3
^{91}Zr	11.868	14.96±0.07	8.89	5.80	26.4±0.3	16.58	2.0±0.3
^{92}Zr	11.812	15.13±0.09	8.86	5.54	26.4±0.3	16.26	1.7±0.3
^{94}Zr	11.68*	14.71±0.10	8.80	5.77	25.9±0.4	16.22	2.0±0.4
^{96}Zr	11.54*	14.22±0.10	8.74	6.05	25.6±0.4	16.2*	2.1±0.4
^{93}Nb	12.059	15.76±0.17	8.83	5.13	26.6±0.3	16.59	2.0±0.3
^{94}Mo	12.32*	16.15±0.10	8.80	4.96	27.1±0.3	16.5*	1.7±0.3
^{96}Mo	12.164	15.86±0.13	8.74	5.04	26.2±0.4	16.5*	2.5±0.4
^{97}Mo	12.146	15.71±0.16	8.71	5.14	26.3±0.4	16.4*	2.2±0.4
^{98}Mo	12.114	15.2±0.3	8.68	5.6	26.0±0.4	16.3*	2.4±0.4
^{100}Mo	12.11*	14.6±0.7	8.62	6.1		16.2*	
^{112}Sn	13.91*	17.22±0.16	8.30	4.99	27.1±0.3	15.9*	2.7±0.3
^{116}Sn	13.860	16.78±0.25	8.20	5.28	27.0±0.4	15.68	2.5±0.4
^{120}Sn	13.701	15.75±0.17	8.11	6.06	25.5±0.3	15.40	3.6±0.3
^{122}Sn	13.63*	15.54±0.09	8.07	6.15	24.6±0.3	15.3*	4.3±0.3
^{124}Sn	13.58*	15.30±0.09	8.02	6.30	24.2±0.3	15.19	4.6±0.3
^{208}Pb	18.834	19.15±0.08	6.75	6.44	27.8±0.2	13.44	4.5±0.2

[a] $E_x(\text{tgt}) = E_x(\text{target}) = 40A^{-1/3}$

* interpolated

the results are given in Table II. The differences, $\Delta E^+ - \Delta E^-$, are consistent with lower-limit estimates of Leonardi[8] of 2 MeV and 4 MeV for ^{120}Sn and ^{208}Pb, respectively.

Unlike the status of the E1 resonance, little is known of the location of M1 strength for heavier nuclei. We assumed $E_x(M1) = 40A^{-1/3}$ and proceeded as with the E1 data to compute isospin splittings. The results are given in Table I. All ΔE^- values fall within a fairly small region around 6 MeV. The average splitting ($\Delta E^-(M1) = 5.3$ MeV) for targets having $T/A=(N-Z)/2A$ between 0.05 and 0.075 corresponds to an optical model symmetry potential of about 85 MeV, close to the expected value.

In conclusion, we can say that the phenomena first observed in the $^{90}Zr(p,n)$ and ^{90}Zr ($^3He,t$) reactions appear to be much more general; they are not restricted to ^{90}Zr. For the peak at the lower E_x, the energy systematics and the earlier information that its angular distribution[1,9] is similar to that of known 1^+ states strongly favor the identification as antianalog of the giant M1 state. For the peak at the higher E_x, the energy systematics point strongly to the interpretation of that peak being the antianalog of the famous E1 giant resonance. This leads directly to the first determinations of the T, T-1 isospin splitting of that resonance. Our data show that the isospin potential has an important tensor component.

Table II. Isospin splittings of the giant E1 resonance and values of the vector and tensor contributions (all in MeV) according to Eqs. 2. Values of ΔE^- are from our work.

Target	ΔE^+	ΔE^-	E_v	E_t	AE_v	AE_t
^{90}Zr	3.9[a]	2.2	0.56	0.010	51	0.90
^{116}Sn	4.0[b]	2.5	0.38	0.0039	44	0.45
^{120}Sn	5.5[b]	3.6	0.44	0.0032	53	0.38
^{124}Sn	6.3[b]	4.6	0.43	0.0020	54	0.25
^{208}Pb	11.2[b]	4.5	0.35	0.0031	73	0.65

[a] Reference 5.

[b] Reference 6, Fig. 13.

1. R.R. Doering, A. Galonsky, D.M. Patterson, and G.F. Bertsch, Physical Rev. Lett. 35, 1691 (1975).
2. A. Galonsky, J.P. Didelez, A. Djaloeis, and W. Oelert, Phys. Lett. 74B, 176 (1978).
3. R. Leonardi, Phys. Rev. Lett. 28, 836 (1972).
4. R.O. Akyuz and S. Fallieros, Phys. Rev. Lett. 27, 1016 (1971).
5. P. Paul, J.F. Amann, and K.A. Snover, Phys. Rev. Lett. 27, 1013 (1971).
6. K. Shoda, Physics Reports 53, 341 (1979).
7. S. Fallieros, p. 401, Proc. Photonuclear Reactions, Asilomar, ed. B.L. Berman (1973).
8. R. Leonardi, Phys. Rev. C14, 385 (1976).
9. D. Ovazza et al., Phys. Rev. C18, 2438 (1978). $\sigma(\theta)$ for ^{90}Zr(He,t) at 80 MeV suggested a mixture of multipolarities, the major one being consistent with a 1^+ assignment.

Level Energies in ^{198}Pt from Proton Inelastic Scattering at 35 MeV

P.T. Deason,* R.M. Ronningen, J.A. Nolen, Jr., C.H. King,** F.M. Bernthal and T.L. Khoo***

As a part of our program to study some of the stable, even Pt nuclei using the (p,p') and (p,t)[1] reactions, we measured the energies of 44 levels to 3.2 MeV excitation energy in ^{198}Pt using the (p,p') reaction at 35 MeV. Of these only six were observed previously,[2,3,4] and precise energies were known for only two.

The scattered protons were detected in the focal plane of the Enge split-pole spectrometer with a delay-line position-sensitive proportional counter, and in a separate experiment, with photographic emulsion plates. In the plate experiment thin (150-200 $\mu g/cm^2$) targets of ^{196,198}Pt and ^{206}Pb were used. The three reactions were recorded on the same plate; only the vertical height of the plate in the focal plane was adjusted. Data were recorded at 43° and 75°. The ^{196}Pt, ^{206}Pb(p,p') reactions were used to produce a position-versus-momentum map of the focal plane, thus calibrating the energies in the ^{198}Pt reaction. These precisely determined energies then were used to calibrate the energies in the counter experiments.

The level energies are given in the table along with spin-parity assignments from angular distribution measurements, the excitation cross sections (at 30°, typically) for most of the levels, and the results of other studies.[2,3,4] The uncertainties in level energies are typically 2 keV below 2.5 MeV and 0.1% in energy above 2.5 MeV.

It has been found convenient[5] to describe the level energy and γ-ray branching ratio systematics in the Pt-Os region by starting with the O(6) limit of the IBA model[6] and breaking this symmetry by introducing a perturbation, the boson quadrupole-quadrupole interaction. We applied this "perturbed O(6)" approach to calculate the level energies in ^{198}Pt. In the figure we show the levels in ^{192,194,196,198}Pt along with the results of the calculation for ^{198}Pt. The striking experimental feature is the grouping of the second 2^+ and 0^+ levels, and the first 4^+ level around a centroid energy slightly larger than twice the energy of the first 2^+ level. This is reminiscent of the SU(5) ("vibrational model") limit predictions of the IBA model. The calculated values do show the proper level sequence but quite different spacings for the second 2^+ and 3^+ levels. It is difficult to understand this behavior because nuclei at the beginning of shells should display SU(5) symmetry and at the end of shells, O(6) symmetry. Gamma decay studies[7] of these

Table 1. States populated in the ^{198}Pt(p,p') reaction.

Present Experiment ^{198}Pt(p,p')			Previous Results[a]	
E_x[b] (MeV)	J^π	$\sigma(30^\circ)$ (μb/sr)	E_x[b] (MeV)	J^π
0.0	0^+	4.92×10^5	0.0	0^+
0.407[c]	2^+	3.24×10^3	0.4072	2^+
0.775	2^+	55.1(40°)	0.775	2^+
0.984	4^+	1.05×10^3	0.991	4^+
1.246(3)	(3^+)	21.9		
1.287	4^+	252	1.305	
1.367	(5^-)	142		
1.445(3)		56.6		
1.502(3)	(7^-)	82.8		
1.657		119		
1.682	3^-	845	1.722	(3^-)
1.722(3)		25.5(40°)		
1.785	(4^+)	150		
1.827(4)				
1.900		113		
1.949				
1.971(4)				
2.000				
2.070		46.6(40°)		
2.100		74.9		
2.120		57.9		
2.155		137		
2.178		52.7		
2.319				
2.339				
2.356				
2.387				
2.441		369		
2.469		49.9		
2.514		108		
2.573		36.3	2.53	
2.611		762		
2.633				
2.666		96.5		
2.726		62.3		
2.782				
2.796		325		
2.826		385		
2.884		38.4		
2.910		38.0		
3.005				
3.018				
3.170(5)				
3.197(5)				

[a] References 2, 3, 4.

[b] Uncertainties in the excitation energies are approximately 2 keV below 2.5 MeV and 0.1% above 2.5 MeV, except where indicated.

[c] Used as calibration point along with the 0.80310, 6.68408, 2.20023, and 2.64790 MeV levels from ^{206}Pb.

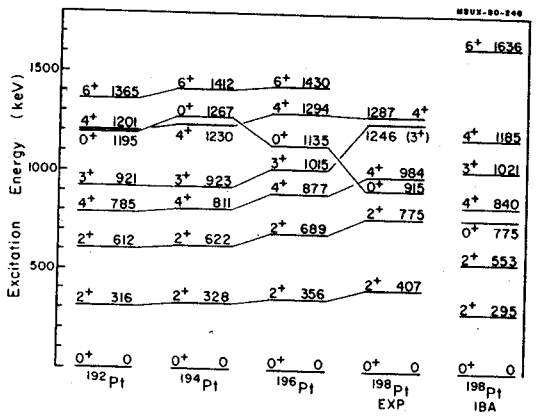

FIG. 1. Systematics of experimentally determined level energies for positive parity states in ^{192,194,196,198}Pt. The data for ^{198}Pt are compared to calculations using the perturbed O(6) limit of the IBA model with κ=0.016 keV.

levels could help us understand better this behavior. A paper on our ^{194,196,198}Pt(p,p') studies is being prepared for publication.

---

* E.I. Du Pont Corp., Savannah River, GA
** Bell Laboratories, Murray Hill, NJ
*** Physics Division, ANL, Argonne, IL

1. P.T. Deason, et al., Phys. Rev. C20, 927 (1979).
2. F.T. Baker, et al., Nucl. Phys. A266, 337 (1976).
3. E.J. Bruton, et al., Nucl. Phys. A152, 495 (1979).
4. Paresh Mukherjee, Nucl. Phys. 64, 65 (1965).
5. R.F. Casten and J.A. Cizewski, Nucl. Phys. A309, 477 (1978).
6. A. Arima and F. Iachello, Annals of Physics 123, 468 (1979).
7. S.W. Yates, private communication, and S.W. Yates, et al., to be published.

Inelastic Scattering on ^{206}Pb at 35 MeV

J.E. Finck, G.M. Crawley, J.A. Nolen, Jr., and S.M. Austin

A high resolution study of inelastic proton scattering is a powerful technique for testing nuclear structure models provided that the bombarding energy is sufficiently high that a direct reaction mechanism can be reasonably assured. Utilizing disperion-matching methods and on-line tuning techniques, exposures have been taken at 35 MeV bombarding energy on nuclear emulsions in the Enge split-pole spectrograph. Results have been obtained at angles between 10° and 90° with a typical resolution of less than 10 keV (FWHM). A spectrum of ^{206}Pb from 1 MeV to 6 MeV excitation energy is displayed below (Fig. 1).

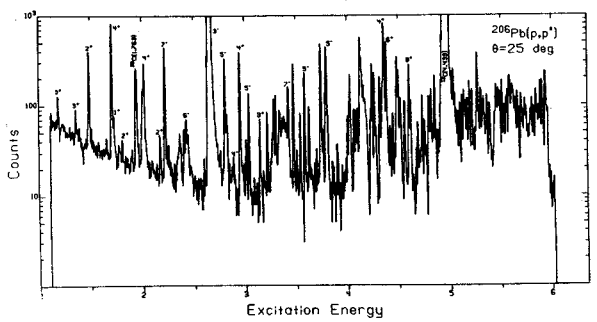

FIG. 1. Spectrum of ^{206}Pb(p,p') observed with nuclear emulsions in the focal plane of the magnetic spectrograph.

The spectrum reveals the collective states of ^{206}Pb as well as many weakly excited levels. A number of unnatural parity states are visible; the 3^+ state at 1.341 MeV of excitation is discernible as well as the 1^+, 6^-, 4^-, and 3^+ states at 1.703, 2.384, 3.242, and 3.122 MeV respectively. The background is small and discrete structure is apparent up to about 6.3 MeV excitation energy.

The angular distributions for natural parity levels have shapes characteristic of particular angular momentum transfers and thus provide an empirical tool to determine unknown angular momentum transfer. A DWBA program using a collective model[1] is being used to analyze these angular distributions. It will be interesting to compare the collective levels in ^{206}Pb to the analogous levels in ^{207}Pb, ^{208}Pb, and ^{209}Bi studied previously.[2]

In applying the shell model to nuclear structure, ^{206}Pb is of considerable interest for studying the behavior of two interacting particles moving in a nuclear potential. Starting with the well-established single hole structure of ^{207}Pb, the levels of ^{206}Pb constitute the first step toward the more complex structure that exists away from closed shells. Calculations based on two interacting neutron holes have been performed for ^{206}Pb and energies and wave functions predicted.[3] With the direct reaction scattering codes available the natural parity state wave functions can be tested. Including the effects of knock-on exchange, and the tensor and spin-orbit two nucleon force will permit a thorough investigation of the theory. Further, observation of the unnatural parity states should allow determination of the tensor and spin-orbit components of the force since scattering into such states is sensitive to these two components especially at higher energies. Calculations are presented in Fig. 2 for the 1.341 MeV 3^+ state. The solid curves represent calculations using a realistic effective interaction derived from nucleon-nucleon potentials.[4] The dashed curves represent calculations using a central interaction in the form of a Serber mixture, a tensor force from the work of Crawley et al.[5] and of Fox and Austin,[6] and a spin-orbit force from the same study

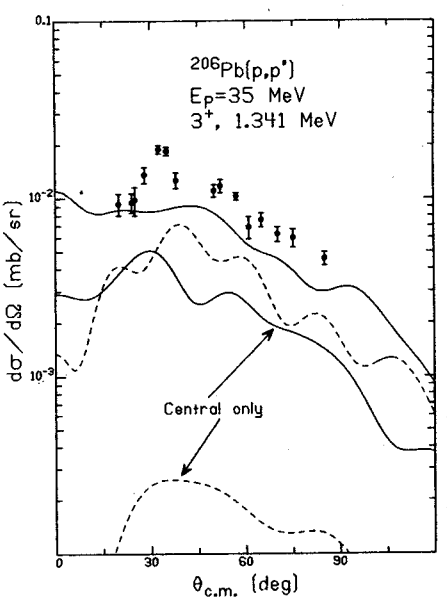

FIG. 2. Experimental and microscopic DWBA angular distributions for the 3^+, 1.341 MeV state in ^{206}Pb. The meaning of the curves is explained in the text.

by Fox and Austin. The shape of the angular distribution is reasonably well predicted, however, the magnitude is slightly underestimated. These calculations also show how the non-central forces enhance the angular distributions.

This study will be completed at Princeton University using a position sensitive wire proportional counter. This part of the experiment will focus on the more strongly excited states, some of which produced tracks too dense to scan at some angles on the photographic emulsions.

---

1. D. Kunz, University of Colorado, unpublished.
2. W.T. Wagner, G.M. Crawley, and G.R. Hammerstein, Phys. Rev. C11, 486 (1975).
3. C.W. Ma and W.W. True, Phys. Rev. C8, 2313 (1973).
4. G. Bertsch, J. Borysowicz, H. McManus, and W.G. Love, Nucl. Phys. A284, 399 (1977).
5. G.M. Crawley, S.M. Austin, W. Benenson, V.A. Madsen, F.A. Schmittroth, and M.J. Stomp, Phys. Letters 32B, 92 (1970).
6. S.H. Fox and S.M. Austin, Phys. Rev. C21, 1133 (1980).

Coulomb Excitation of ^{142,144,146,148,150}Nd

A. Ahmed,* R.M. Ronningen, G.L. Bomar,* H. Crowell,* J.H. Hamilton,* H. Kawakami,* C.F. Maguire,* W.G. Nettles,* R.B. Piercey,* A.V. Ramayya,* R. Soundranayagan,* and P.H. Stelson**

The stable Nd nuclei are interesting because they span a large range of deformation, from the spherical ^{142}Nd(N=82) to the deformed ^{150}Nd(N=90). We are studying this transition from spherical to deformed intrinsic shapes by measuring absolute B(E2) and B(E3) values of low-lying ($\lesssim$1.5 MeV) states with $J^\pi=2^+$ and 3^- using Coulomb excitation with α particles. Also, we are extracting values of E4 matrix elements (M_{04}) where possible.

The Coulomb excitation of ^{142,144,146}Nd ^{148,150}Nd was studied by detecting α particles scattered into 150°, using a position-sensitive proportional counter in the focal plane of the Enge split-pole spectrometer at ORNL. Beams of 10-11 MeV α particles were supplied by the ORNL EN tandem Van de Graaff. We observe the excitations of the first $J^\pi=2^+$ state in all isotopes, the first $J^\pi=3^-$ state in all except ^{142}Nd, the first 4^+ state in ^{146,148,150}Nd, and the second and third 2^+ states in ^{148,150}Nd. Our analysis of the experimental excitation probabilities is being carried out using semi-classical and quantum mechanical Coulomb excitation calculations. For ^{150}Nd, our preliminary results yield values of B(E2)= 2.82(4)e^2b^2 and M_{04}=0.25 (12)eb^2 for the ground band 2^+ and 4^+ states. Also, B(E2)=0.015(3)e^2b^2 for the $J^\pi K=2^+0$ state at 851 keV, B(E3)=0.18 (3)e^2b^3 for the 3^- state at 932 keV, and B(E2)= 0.076(5)e^2b^2 for the 2^+2 state at 1062 keV.

Because the extracted transition probabilities are sensitive to the many matrix elements which go into the calculations (and thus possibly the nuclear model from which these might be obtained) we plan to use matrix elements deduced from γ-ray studies and lifetime measurements (eg. Ref. 1), when possible. When this is not possible, matrix elements from the IBA model[2] will be used. This model adequately describes the level energies and observed transition probabilities in the neighboring Sm isotopes.[3]

---

* Vanderbilt University, supported in part by a grant from U.S.D.O.E.
** ORNL, operated by Union Carbide for the U.S.D.O.E.

1. S.W. Yates, Noah R. Johnson, L.L Riedinger, and A.C. Kahler, Phys. Rev. C17, 634 (1978).
2. A. Arima and I. Iachello, Phys. Rev. Lett. 35, 1069 (1975).
3. A. Arima and I. Iachello, Ann. Phys. (NY) 115, 325 (1978).

Multipole Moments of ^{232}Th and ^{234,236,238}U from Proton Inelastic Scattering

R.C. Melin, R.M. Ronningen, J.A. Nolen, Jr., G.M. Crawley, C.H. King, J.E. Finck and C.E. Bemis, Jr.*

The deformed actinide nuclei that are accessible to scattering experiments afford good tests of theories for the ground state deformation, fission barrier properties, and single particle structure of this region. The purpose of our study is to use proton inelastic scattering and a multipole moment technique to make more unambiguous comparisons of results from Coulomb excitation, electron scattering, and α-particle scattering, as well as the comparison of experimental to theoretical results for this region. The proton is a simple probe and because of the strong p-n interaction, the (p,p') reaction is potentially complimentary to electromagnetic interactions in its sensitivity to the neutron distribution.

The inelastic scattering reactions were measured using 35 MeV protons from the MSU Cyclotron with scattered protons detected in the focal plane of the Enge split-pole spectrometer by a delay-line position-sensitive proportional counter. Tetra-fluoride, rolled, and isotope-separated targets were used. The analysis of the data follows closely our earlier study.[1] We have increased twofold the number of data points for ^{232}Th and ^{238}U, increased the angular range and have added ^{234,236}U. Briefly, the angular distributions were analyzed using a deformed optical model potential (DOMP). The coupled channels calculations, incorporating the axially symmetric rotor model, included grid and gradient searches on the well depths, diffusenesses, and deformation parameters β_2, β_4, and β_6. The data for ^{232}Th and ^{234,236,238}U are shown in Figures 1, 2, 3, and 4 along with coupled channels calculations. From the DOMP parameters we calculate the multipole moments of the real part of the DOMP.[2,3] These are normalized to facilitate comparisons with the electromagnetic moments from Coulomb excitation[4] and electron scattering.[5] Similarly, we compute moments from the DOMP parameters for alpha particle scattering.[6,7]

A comparison of the quadrupole (q_2) and hexadecapole (q_4) moments from (p,p'), (α,α'), (e,e') and from Coulomb excitation, for ^{232}Th, ^{234,236,238}U is shown in Fig. 5, along with predictions from a microscopic model.[8] Our preliminary values of q_2 and q_4 from (p,p') follow the trends of those from Coulomb excitation but are 5-8% smaller for q_2 and 15-30% smaller for q_4 (except for ^{238}U). It is difficult to assess the apparent, systematic differences between the experimental results for the (p,p') and Coulomb excitation. They may arise from real differences between proton and neutron

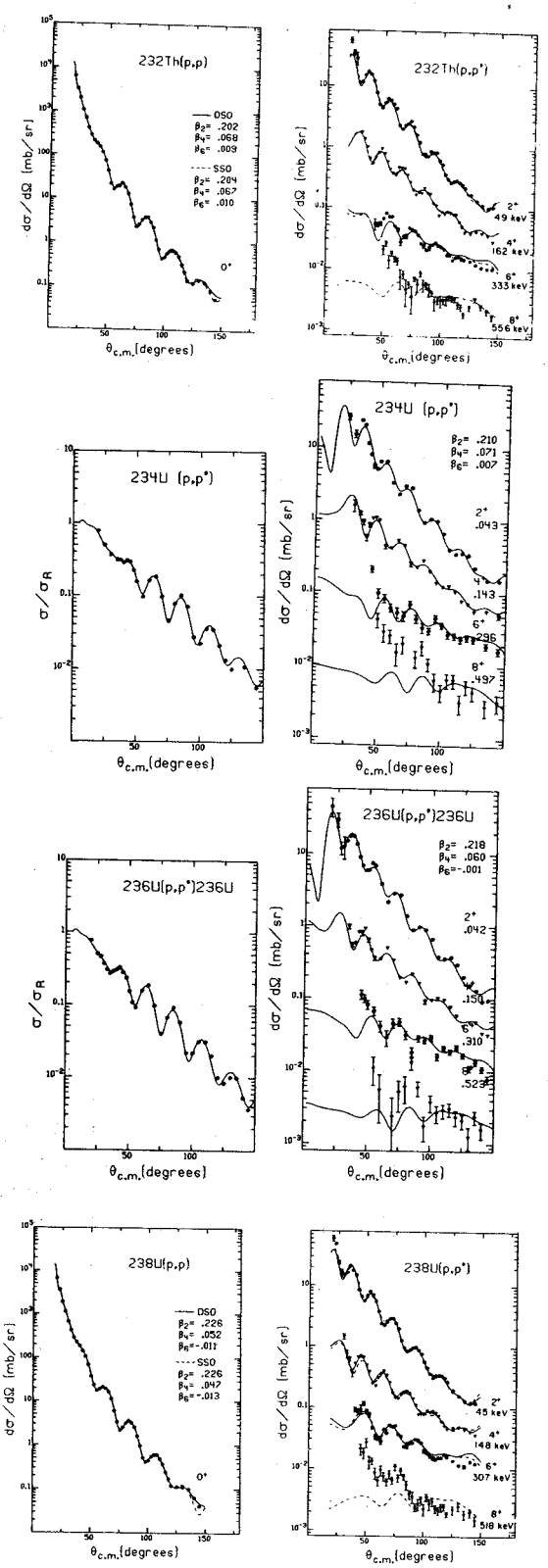

FIGS. 1, 2, 3 and 4. Angular distributions of elastic (left) and inelastic (right) proton scattering at 35 MeV from ground-band states in ^{232}Th and ^{234,236,238}U. The lines result from coupled channels calculations. For ^{232}Th and ^{238}U the solid lines are calculated using the deformed spin-orbit interaction DSO), and the dashed lines, using the spherical spin-orbit interaction (SSO). For ^{234,236}U only SSO calculations are shown.

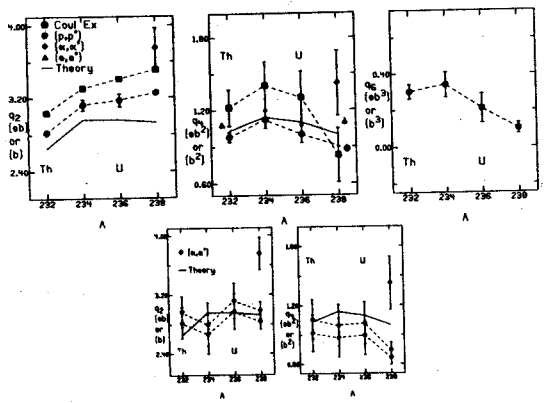

FIG. 5. Comparisons of values of q_2 and q_4 from scattering experiments compared to theoretical calculations for ^{232}Th, ^{234,236,238}U. For ^{238}U, the largest values of q_2, q_4 from (α,α') are deduced from Ref. 7. We used both DOMP sets in Ref. 6; the deeper potential yields smaller q_2, q_4 values. Values of q_6 are also shown.

moments, density-dependent effects in the reaction, or from the phenomenological nature of our analysis. Hartree-Fock calculations[9] show differences ($\leq$ 5%) between proton and neutron moments but of opposite sign from what we observe. For equal proton and neutron deformations, calculations[10] of density-dependent effects predict larger potential moments than charge moments.

The (p,p') values for q_2 are closer to, in general, the values from Coulomb excitation than are the values from (α,α'). The theoretical values reproduce nearly the trends, but not the magnitudes of the Coulomb excitation and (p,p') values for q_2. Also, the decrease in hexadecapole strength in ^{238}U compared to ^{234,236}U, seen by the Coulomb excitation, (p,p') and (α,α') reactions, is not reproduced.

We are also investigating the influence of the β_6 deformation. Our preliminary finding is that somewhat better fits to the data are achieved by including small values of β_6. For ^{232}Th and ^{234}U, $\beta_6 \simeq +0.010$, for ^{236}U, $\beta_6 \simeq 0.000$, and for ^{232}U, $\beta_6 \simeq -0.013$, i.e. a trend from position to zero and then to negative values as particles are added. This is similar to the variation of β_4 values from the light to heavier rare earth nuclei, as explained qualitatively by Bertsch.[11] The hexakontattetarapole moments (q_6) also shown in Fig. 5 have values of 0.30, 0.34, 0.21, and 0.10 b^3, respectively.

1. C.H. King, J.E. Finck, G.M. Crawley, J.A. Nolen, Jr., and R.M. Ronningen, Phys. Rev. C 20, 2084 (1979).
2. R.S. Mackintosh, Nucl. Phys. A266, 379 (1976).
3. G.R. Satchler, J. Math, Phys. 13, 1118 (1972).
4. C.E. Bemis, Jr. et al., Phys. Rev. C 8, 1466 (1973).
5. T. Cooper et al., Phys. Rev. C 13, 1083 (1976).
6. P. David et al., Z. Physik A278, 281 (1976).
7. D.L. Hendrie, Phys. Rev. Lett. 31, 478 (1973).
8. B. Nerlo - Pomorska, Nucl. Phys. A259, 481 (1976); Electric Multipole Moments of Atomic Nuclei, Report No. 538, Institute of Nuclear Research, Warsaw, Poland, 1974.
9. J.W. Negele and G. Rinker, Phys. Rev. C 9, 1499 (1977), and J.W. Negele, private communication.
10. J.K. Hamilton and R.S. Mackintosh, J. Phys. G3, L19 (1977), and 4 579 (1978).
11. G.F. Bertsch, Phys. Lett. 26B, 130 (1968).

A Remark on Y_{60} Deformations of Rare-Earth and Actinide Nuclei

R.M. Ronningen

While the presence of intrinsic nuclear deformations of quadrupole ($\lambda=2$) and hexadecapole ($\lambda=4$) order is quite well established in the deformed rare-earth and actinide regions there have been very few experimental or theoretical studies of the 2^6-pole (hexakontattetarapole) order deformation. One interesting, basic but quite open question is the expected trend of this deformation across deformed regions.

Some time ago Bertsch[1] proposed a simple picture of why intrinsic moments should arise and how they should vary for nuclei within a major shell. He was able to explain the existence of positive values of hexadecapole moments (Q_4) at the beginning of a deformed region and negative values at the end of the region. We have extended this picture to hexakontattetarapole order. It predicts positive values of the moment at the beginning and end of the deformed region, and negative values in the middle.

To review how well Bertsch's picture is substantiated by experiment for $\lambda=2$ and 4, and to test its extrapolation to $\lambda=6$, we display the predictions for $\lambda=2$, 4, and 6 and experimental data for the rare-earth region in Fig. 1, and for the actinide region in Fig. 2. In both regions the magnitudes of the predictions are normalized to the data, individually for each moment. For the rare-earth region the experimental data on Q_2 and Q_4 come from Coulomb excitation studies.[2] The Q_6 moments come from the application of Satchler's theorem[3,4] using (α,α')[5] and (p,p') reaction[6] coupled channels optical model parameters.

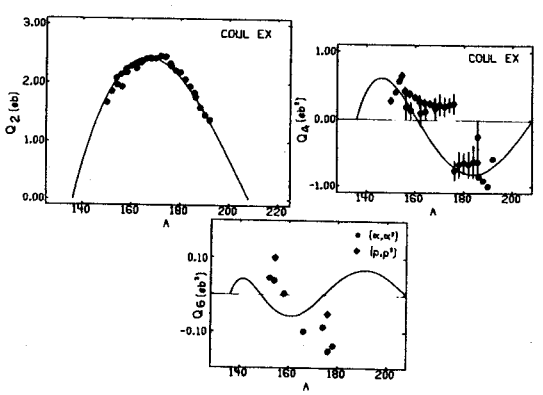

FIG. 1. Experimental values of Q_2, Q_4, and Q_6 moments in the rare-earth region. The trends compared to predictions (solid lines) by Bertsch's model.

In the actinide region, where data from scattering experiments are sparse because of target considerations, the Q_2 and Q_4 moments for the even-A nuclei are from Coulomb excitation[7] and electron scattering experiments,[8]

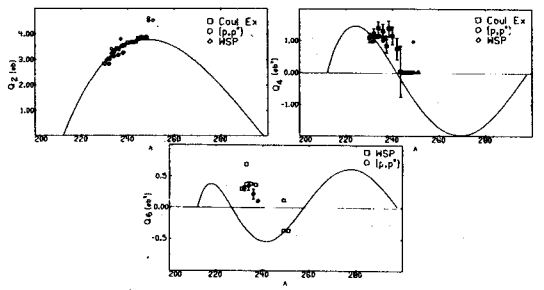

FIG. 2. Experimental and estimated values of Q_2, Q_4, and Q_6 moments in the actinide region. The trends are compared to predictions (solid lines) by Bertsch's model.

and those deduced from (α,α')[9,10] and (p,p')[11] optical model parameters. For some odd-A nuclei the Q_2, Q_4, and Q_6 moments were estimated from the deformation parameters obtained from application[12] of the deformed shell model to low-excitation energy levels of these nuclei. The Q_6 values from our (p,p') studies are also shown.

There are at least two features to note. First, the variations of Q_2 and Q_4 values across both deformed regions are qualitatively described by Bertsch's model, as has been noted some time ago for the rare-earth region. The apparent quantitative disagreement in the maxima and crossing points of Q_4 presumably is because the simple picture neglects shell, surface, and Coulomb energy effects. Second, although the data are few, there is an indication that the first transition of the Q_6 moment, from positive to negative values, is observed in the vicinity of A=160 and A=240, in the rare earth and actinide nuclei, respectively. This is reflected in the apparent sign change of the β_6 deformation in the Th and U nuclei we studied using the (p,p') reaction.[11] And, for these nuclei, such a behavior is expected in or near these nuclei as predicted by Bertsch's model, that is, near the masses where Q_4 values have their largest, positive values.

Finally, we note that to our knowledge there is only one microscopic calculation of β_6 values for a series of nuclei. These values[13] are for the rare earth region and are displayed in Fig. 3. The predicted changes in sign of β_6, at A≈160 and at A≈190, give credence to the extention of Bertsch's picture to $\lambda=6$ order and lead us to expect that microscopic calculations of Q_6 (when available) in both deformed regions should follow these trends. Such calculations are needed for the actinide region as well as more extensive experimental evidence for $\lambda=6$ shape components in both regions.

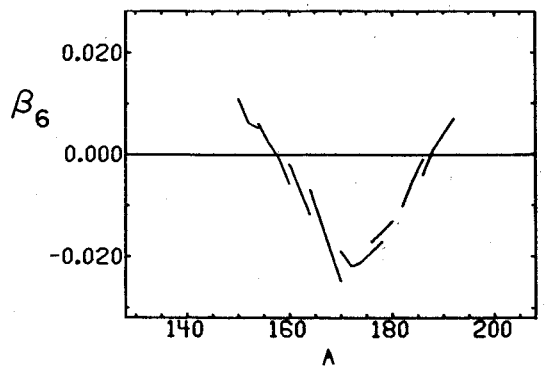

FIG. 3. Microscopic calculations of β_6 deformations in the rare-earth region (from Ref. 13).

1. G.F. Bertsch, Phys. Lett. 26B, 130 (1968).
2. For a survey of these, see R.M. Ronningen et al., Phys Rev. C16, 2208 (1977).
3. D.L. Hendrie et al., Phys. Lett. 26B, 127 (1968).
4. M.L. Barlett et al., Phys. Rev. C22, 1168 (1980).
5. R.S. Mackintosh, Nucl. Phys. A266, 379 (1976).
6. G.R. Satchler, J. Math. Phys. 13, 1118 (1972).
7. C.E. Bemis, Jr. et al., Phys. Rev. C8, 1466 (1973).
8. T. Cooper et al., Phys. Rev. C13, 1083 (1976).
9. P. Daivd et al., Z. Phyzik A278, 281 (1976).
10. D.L. Hendrie, Phys. Rev. Lett. 31, 478 (1973).
11. R.C. Melin et al., this annual report.
12. R.R. Chasman, Phys. Rev. C14, 1935 (1976).
13. S.G. Nilsson et al., Nucl. Phys. A131, 1 (L969).

Spin Determination of Deep Hole States from ($\vec{p}$,d) Reactions

J. Kasagi, G.M. Crawley, S. Gales,* E. Gerlic,* D. Friesel,** and A. Bacher**

In previous studies of deep hole states in medium mass nuclei, the ℓ value of the transferred particle has been determined by angular distribution measurements. The j of the deep hole states, however, has been assigned only on the basis of theoretical expectations of the positions of particular orbits. It is therefore highly desirable to determine the j unambiguously.

A strong j dependence is expected from DWBA calculations for the analyzing power (Ay) of ($\vec{p}$,d) reactions even with rather high incident energies. The Ay measurement in ($\vec{p}$,d) reactions on some light nuclei at E_p = 65 MeV has shown the experimental j dependence of the analyzing power.[1] Spin determination of deeply-bound proton hole states has been done by Ay measurements in ($\vec{d}$,^{3}He) reactions.[2] Measurements of the (p,d) reaction at 90 MeV on a series of Sn isotopes showed that the deep hole states near 5 MeV and 8 MeV excitation energy, were strongly excited.[3]

Differential cross sections and analyzing powers have therefore been measured for ($\vec{p}$,d) reactions on ^{90}Zr, ^{120}Sn and ^{208}Pb using a 90 MeV polarized proton beam from the Indiana University Cyclotron. The beam polarization was measured frequently and was found to be about 70%. The spin direction of the incident beam was flipped automatically every minute during the data taking runs to reduce systematic errors. The outgoing particles were detected by two Si/Ge detector telescopes and were identified using hard wired particle identification boxes to minimize computer dead time. The energy resolution was about 100 keV FWHM.

The measured Ay for several low-lying states in ^{89}Zr and ^{119}Sn are shown in Fig. 1. The Ay for the low-lying $p_{1/2}$ (0.595 MeV) and $p_{3/2}$ (1.1 MeV) states in ^{89}Zr are completely out of phase. The Ay for the $g_{9/2}$ (g.s., ^{89}Zr) and $h_{11/2}$ (0.09 MeV, ^{119}Sn) states with j=ℓ+1/2 are very similar with a dip at about 20° and increase rather steadily with angle beyond 20°. On the other hand, the Ay for the $f_{5/2}$ (1.46 MeV, ^{89}Zr) and $g_{7/2}$ (0.79 MeV, ^{119}Sn) states with transferred j=ℓ-1/2 have negative values at forward angles and smaller values than the j=ℓ+1/2 cases.

Distorted wave Born approximation (DWBA) calculations have been carried out using the code DWUCK with finite range corrections. Optical potentials used in the calculation are almost the same as in ref. 4 and ref. 5 except the Vs.o. of the proton channel which is slightly modified to obtain better fits to the data.

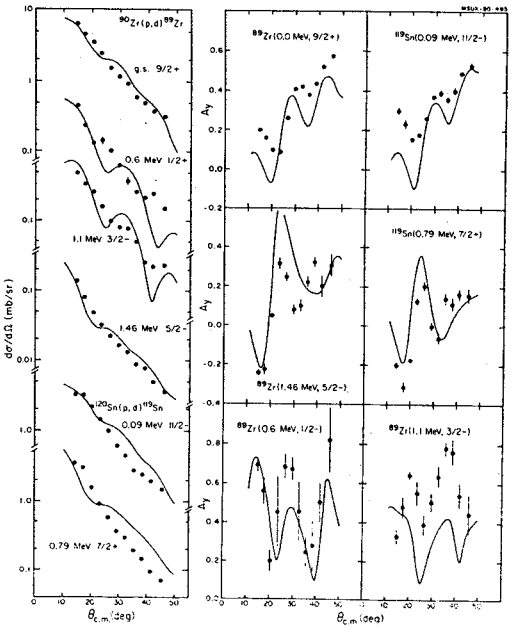

FIG. 1. Experimental and calculated differential cross sections and analyzing powers for the transitions indicated in the figure.

The calculated angular distributions of the cross sections reproduce the experimental angular distributions rather well for all the transitions. The spectroscopic factors of the low-lying states deduced in the present analysis are also in good agreement with the previously reported values.

The calculated Ay's are shown as solid lines in Fig. 1. Reasonable fits are obtained for the $g_{7/2}$ (0.79 MeV, ^{119}Sn), the $g_{9/2}$ (g.s., ^{89}Zr) and the $h_{11/2}$ (0.09 MeV, ^{119}Sn) transitions. However, for the $p_{3/2}$ (1.1 MeV, ^{89}Zr) transition, somewhat worse fits are obtained. The calculated Ay for the analog states around 9 MeV excitation in ^{89}Zr are also in good agreement with experiment.

The Ay of the broad structure near 5 MeV excitation energy in ^{119}Sn is shown in Fig. 2. It is similar to other j=ℓ+1/2 transitions and is compared to the ground state of ^{89}Zr with a known j of 9/2 in Fig. 2a (solid line). Considering the small angle shifts which come from the momentum transfer differences, the two measurements agree very well. This provides a unique spin determination of 9/2 for the broad structure of ^{119}Sn. In Fig. 2b the results of a DWBA calculation are also shown. The solid curve is the calculation for the $g_{9/2}$ transition and the dotted curve for the $g_{7/2}$ transition. The $g_{9/2}$ calculation gives a good fit to the

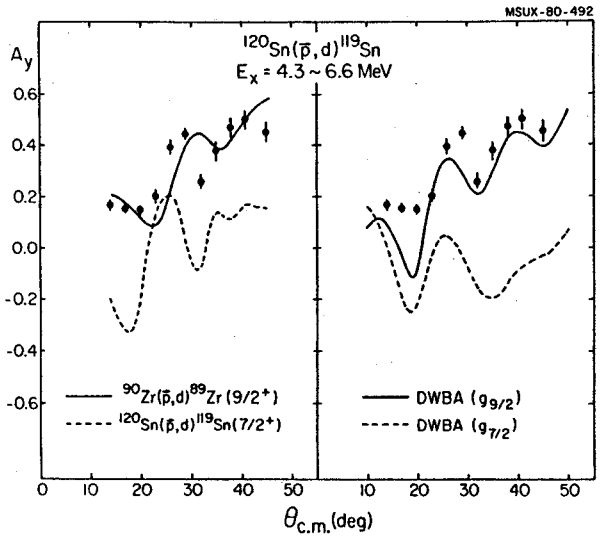

FIG. 2. Analyzing power of the broad structure near 5 MeV excitation energy in ^{119}Sn.

data except at forward angles, where the calculation cannot reproduce the data for the low-lying state. The $g_{7/2}$ calculation is quite dissimilar to the data. This comparison gives a further confirmation of the spin assignment of this neutron hole state.

---

* IPN, BP No. 1 - 91406 Orsay, France.
** IUCF, Indiana University, Bloomington, IN 47405.

1. K. Hosono et al., Proc. 1978 INS International Symposium on Nuclear Direct Reaction Mechanism, ed. M. Tanifuji and K. Yazaki (INS, Univ. Tokyo, 1979), p. 115.
2. A Stuirbrink et al., Contribution for International Symposium on Highly Excited States in Nucleus, Ohsaka, 1980.
3. G.M. Crawley, in Structure of Medium-Heavy Nuclei 1979, ed. Demokritos Group, Athens (The Institute of Physics, 1980) p. 127.
4. P. Schwant, private communication.
5. G. Duhamel, L. Marcus, H. Langevin-Joloit, J.P. Didelez, P. Narboni and C. Stephan, Nucl. Phys. A174 (1971) 485.

Pairing Model Predictions for the Cd(p,t) Reactions

G.M. Crawley, W. Benenson, G. Bertsch, S. Gales, D. Weber and B. Zwieglinski

In order to gain further insight into the structure observed in two neutron pickup experiments on the tin isotopes,[1,2,3] a similar experiment was carried out on the even-even isotopes of cadmium viz. ^{106}Cd, ^{110}Cd, ^{112}Cd, ^{114}Cd and ^{116}Cd using the 42 MeV proton beam from the K50 MSU cyclotron. The tritons were detected in the focal plane of the Enge split pole spectrograph using a position sensitive proportional counter backed by a plastic scintillator. A discussion of the levels observed in ^{104}Cd was given in the 1978-79 Annual Report.

Triton spectra measured at a laboratory angle of 20^{o} are shown in Fig. 1. Broad structure is observed in all the cadmium isotopes although there appears to be somewhat more structure in the cadmium spectra than in the tin spectra particularly for the lighter cadmium nuclei. In the ^{104}Cd spectra it is possible to resolve individual levels or small groups of levels. The excitation energy of the peak of the broad structure increases with the target mass. Another important feature observed in the cadmium spectra is the appearance of a second broad bump at an even higher excitation energy. This second peak is marked with an arrow in the spectra in Fig. 1.

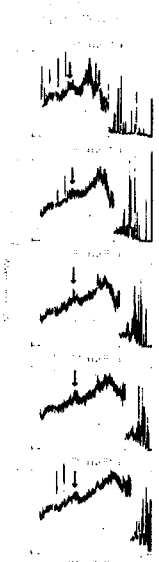

FIG. 1. Triton spectra from (p,t) reactions on the even even cadmium isotopes. The arrow points to the higher energy bump which may correspond to pickup from two deep orbits (see text).

The excitation energies of these features in the cadmium spectra are plotted against the target mass in Fig. 2 together with the values observed in the tin isotopes. In the cases

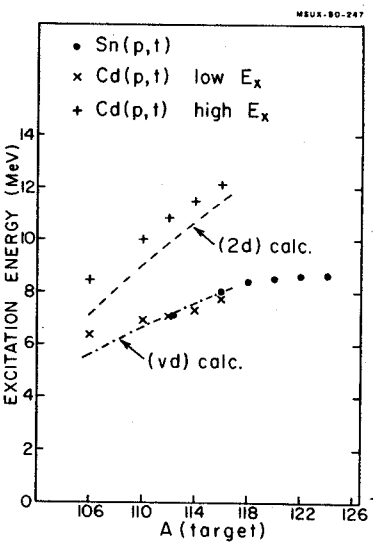

FIG. 2. Excitation energy for broad features observed in triton spectra on even even cadmium and tin isotopes. The dashed-dot line is a prediction assuming one particle comes from a valence orbit and one from a deep orbit (v+d model). The dashed line is a prediction assuming both particles come from deep orbits (2d model).

where the target mass for cadmium and tin are the same (A=112 and 116) the value of the excitation energy for the lowest lying bump in the cadmium isotopes matches very closely the value for the tin isotopes. In general, the values of the excitation energies of the lowest energy feature show a smooth trend from cadmium to tin. In contrast, the excitation energy of the higher excited state in the cadmium isotopes increases much more rapidly with A than the lower energy bump.

Angular distributions have been extracted for the two broad features observed in the $^{106}Cd(p,t)^{104}Cd$ reaction but as was also noted for the tin case, these distributions do not distinguish different structures (Fig. 3). Even though the higher energy feature must contain ℓ=0 strength if it arises from pickup of particles from the same deep orbit, and the lower excitation energy bump does not, the ℓ=0 strength does not dominate the cross section. Both angular distributions appear to be incoherent mixtures of different ℓ transfers similar to the cases measured in the tin isotopes.

A qualitative understanding of the energy systematics in the tin isotope has been obtained using a simple pairing model for the two cases (1) when both neutrons are picked up from deep orbits (the 2d case) and (2) where one neutron is picked up from a valence orbital and one

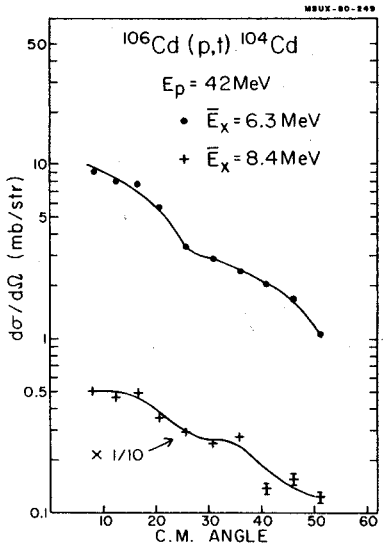

FIG. 3. Angular distributions for broad features observed in ^{106}Cd(p,t) at E =42 MeV. The solid lines are only to guide the eye.

from a deep orbital. (The v+d case) The details are given in Refs. 3 and 4 and the energetics are summarized in Table I.

In the case of the Sn isotopes, the conclusion was reached that the broad bump around 8 MeV excitation energy had a substantial component of the (v+d) configuration.

The simple pairing model for the excitation energy was also applied to the cadmium isotopes using the same values of V_{dd}(-1.7 MeV) and Δ(1.4 MeV). The (v+d) calculation is shown as a dot-dashed line in Fig. 2 which matches very well the magnitude and the variation with A of the excitation energy of the lowest energy feature. The implication is that this first bump corresponds to the same general configuration as was observed in the tin isotopes with one particle coming from a deep orbit and one from a valence orbit. The (2d) calculation, on the other hand, shown by a dashed line in Fig. 2 is lower by about 1 MeV than the experimental values for the higher energy bump but has a very similar slope. In fact, a choice of V_{dd} of about -0.7 MeV would bring the prediction into good agreement in both magnitude and slope with the measured values. This suggests that the second feature observed in the cadmium isotopes may correspond to picking up two particles from deep orbits.

1. G.M. Crawley, W. Benenson, D. Weber, and B. Zwieglinski, Phys. Rev. Letters 39, 1451 (1977).
2. G.M. Crawley, S. Gales, D. Weber, B. Zwieglinski, W. Benenson, D. Friesel, A. Bacher, B.M. Spicer, Phys. Rev. 22C, 316 (1980).
3. G.M. Crawley, Paper presented at Osaka Meeting May 1980.
4. G.M. Crawley, W. Benenson, G. Bertsch, S. Gales, D. Weber and B. Zwieglinski, to be published.
5. R.A. Broglia and D.R. Bes, Phys. Letters 69B, 129 (1977).

Table I.

State	Excitation Energy Formula	Numerical*
Single deep hole (1d)	$e_d - e_v \simeq (\varepsilon_F - \varepsilon_d) - \Delta$	5.4 MeV
Deep hole pair (2d)	$2e_d + V_{dd} \simeq 2(\varepsilon_F - \varepsilon_d) + V_{dd}$	11.9 MeV
Valence hole plus deep hole (v+d)	$e_d + e_v + V_{vd} \simeq (\varepsilon_F - \varepsilon_d) + \Delta$	8.2 MeV

*Numerical: For target of A=118.
Pairing gap, $\Delta \simeq 1.4$ MeV, from average odd-even mass difference.
Interaction energy between particles in deep orbits, V_{dd} = -1.7 MeV, from ref. 5
$\varepsilon_F - \varepsilon_d$ = 6.8 MeV, from empirical (1d) energy

Energy Levels in ^{60}Ni from a Study of the ^{59}Ni(d,p) Reaction

M.S. Curtin, R.M. Ronningen, J.A. Nolen, Jr., R.C. Melin,* S. Raman** and H. Nann***

In the previous annual report we presented the experimental detail and preliminary results of a study of ^{60}Ni using the ^{59}Ni(d,p) reaction at 20 MeV. The nuclear emulsion plate containing the high excitation energy level information at 10° has now been scanned and analyzed for peak positions and yields. The low and high excitation energy plate data at 10° are shown in Fig. 1. The horizontal axis are labeled by excitation energies. These levels have been observed previously in (n,γ) and (p,p') reactions.[1] The (n,γ) reaction results are being used to calibrate the excitation energies in our plate data so that precise level energies for all observed levels in both our plate and counter data can be obtained. The levels excited in the (d,p) reaction will then be compared to those excited in the (n,γ) and (p,p') reactions. The counter data have been analyzed but not yet collated with the plate data.

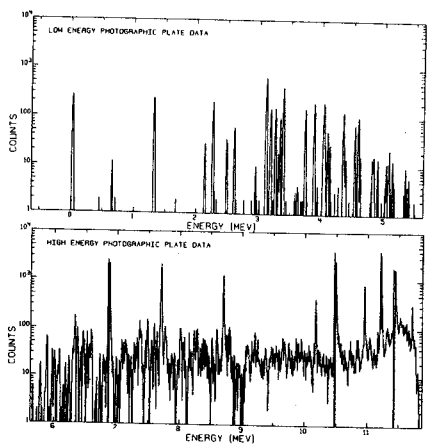

Fig. 1

Data were also collected at 30° and 40° for the ^{59}Ni(d,d) reaction. By comparing the elastic yields to optical model calculations the target thickness was obtained so that absolute cross sections can be known for the angular distribution data. DWBA calculations will be performed and spectroscopic factors will be extracted.

---

* Bell Laboratories, Murray Hill, NJ.
** ORNL, Oak Ridge, TN.
*** Indiana University, Bloomington, IN.

1. S. Raman et al., to be published.

Nuclei Far from Stability in the Light Tin Region

D.C. Coyle and Wm. C. McHarris

We have been gradually working our way toward the doubly-cloud-shell nucleus ^{100}Sn in our search for new short-lived nuclei far from stability. From systematic trends in this region, half-lives of the order of a few seconds can be expected, well within the experimental range of HeJRT techniques. Reaction cross-sections using the evaporation code ALICE[1] had us to expect a reasonable probability for observing ^{104}Sn - ^{106}Sn with beams from the old 50 MeV MSU cyclotron.

A 90% enriched ^{106}CdO target pressed onto a 2-mil Al foil backing was bombarded with 40-75 MeV ^{3}He beams. The resulting activities were transported quickly (within 1 sec) by the HeJRT system[2] to a low-background area atop the shielding for counting. γ-γ coincidence data was obtained with various combinations of small and large, planer and coaxial Ge(Li) detectors and at times NaI(Tl) detectors. These were stored on magnetic tape in γ-γ time mode, using standard "megachannel" coincidence techniques and later sorted off line.

Preliminary analyses of these experiments are indicated by the accompanying skeletal decay schemes. With extensive γ-ray singles spectra (several examples also shown), we were able to combine the γ-γ coincidence data with excitation portions. The results are not complete, but, taken together with anticipated heavy-ion produced activities within the coming year, it should be possible to complete an extensive survey of In, Cd, and Ag, as well as Sn nuclei in this general nuclear region.

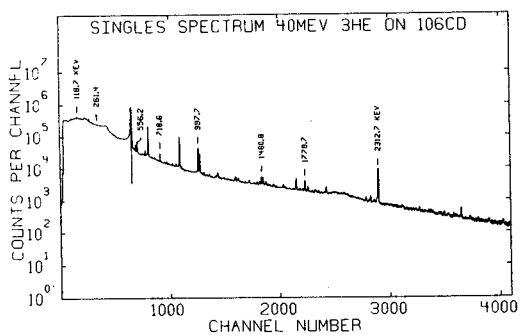

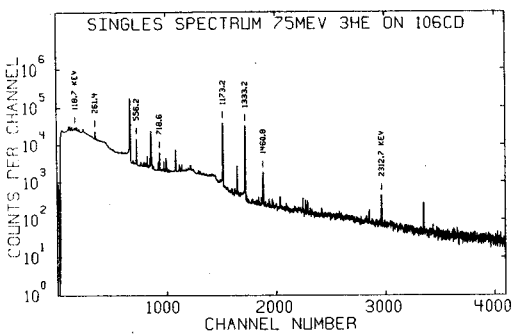

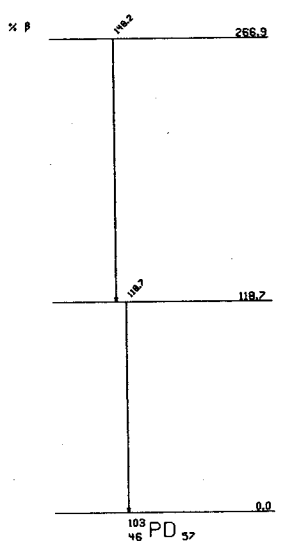

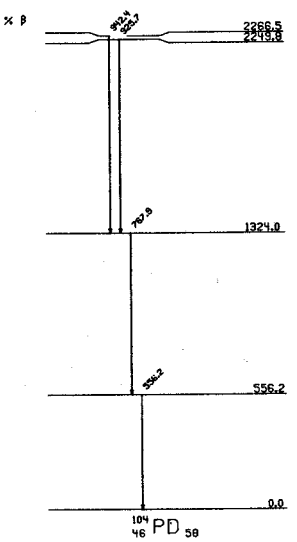

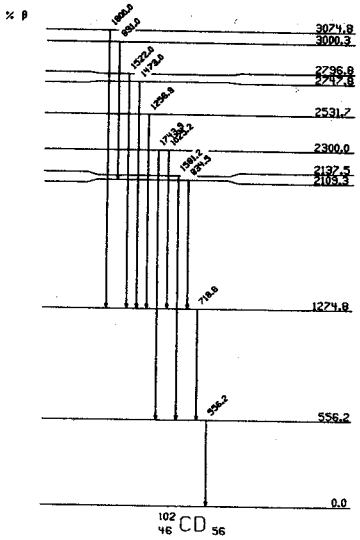

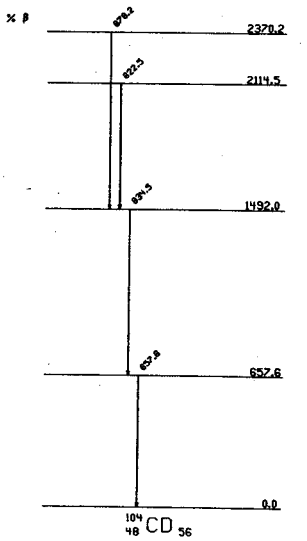

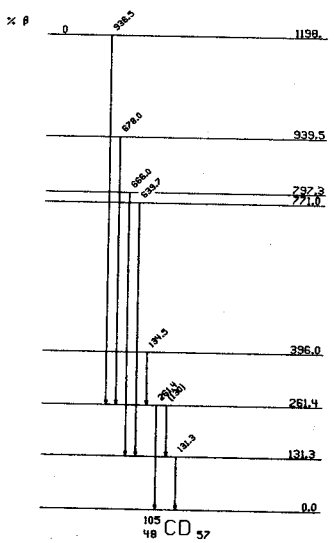

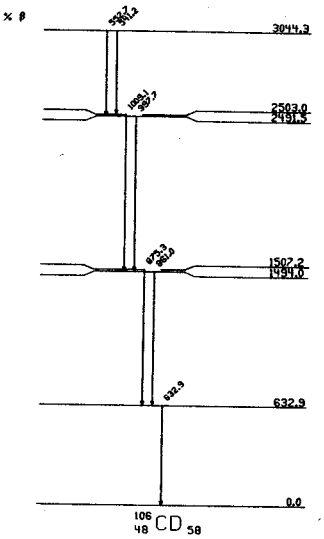

1. M. Blann and F. Plasil, ALICE: A Nuclear Evaporation Code, U.S. Atomic Energy Commission Report No. C00-3293-10, 1973.
2. K.J. Kosanke, M.S. Edmiston, R.A. Warner, R.B. Firestone, and Wm. C. McHarris, Nucl. Instr. Meth. 17, 78 (1975).

In-Beam γ-Ray Spectroscopy of Excited States in Odd-Mass N=80 Nuclei

R. Aryaeinejad, W.H. Bentley, R.B. Firestone, P.M. Walker, and Wm. C. McHarris

One of the more interesting regions of the nuclidic chart for current study is the region immediately below the N=82 closed shell. Here long chains of isotones are amenable to study, encompassing both neutron-excess and neutron-deficient nuclei; a wealth of M4 and other isomers is available; and a large number of targets is available for cross-comparison in various in-beam experiments. The neutron-deficient N=80 isotones are among the most interesting of these nuclei because, although they lie close to the major closed shell, they also lie at a considerable distance from stability. Thus, they are transitional nuclei: they contain many well-defined shell-model states, but they lie near the onset of deformation, so many of their higher-lying states can be characterized not only as multiple particle states, but also as (deformed) collective states. Also, the juxtaposition of the $h_{11/2}$ shell-model state with various low-spin states leads to a wealth of both high and low-spin states in these nuclei.

The level structures of ^{143}Eu, ^{141}Pm, and ^{139}Pr have been investigated in this lab during the past few years, using the techniques of in-beam γ-ray spectroscopy.[1] Levels in ^{143}Eu were populated by the (p,2nγ) reaction only, whereas levels in ^{141}Pm and ^{139}Pr were populated by both the (p,2nγ) and (α,4nγ) reactions. These supplement and complement other previous studies of states in these same nuclides excited by β^+/ε decay. The in-beam experiments, especially the (α,4nγ) experiments, also tended to excite higher-spin states than those known from the existing β-decay data.

High-resolution singles γ-ray sepctra, excitation reactions for the various γ rays, prompt and delayed γ-γ coincidences, and angular distributions of the γ rays in these nuclei were measured in an effort to elucidate their level schemes in as much detail as possible. The accompanying figures illustrate the results from a few of the experiments. (For more details, see (1) or the publications resulting from this work.[2-4] In Fig. 1 we show a singles γ-ray spectrum from the ^{144}Sm(p,2nγ)^{143}Eu reaction. In Fig. 2 we show a sampling of the γ-γ coincidence results from the ^{141}Pr (α,4nγ)^{141}Pm reaction. And in Fig. 3 we show a sampling of the angular distribution results from the ^{139}La(α,4nγ)^{139}Pr reaction.

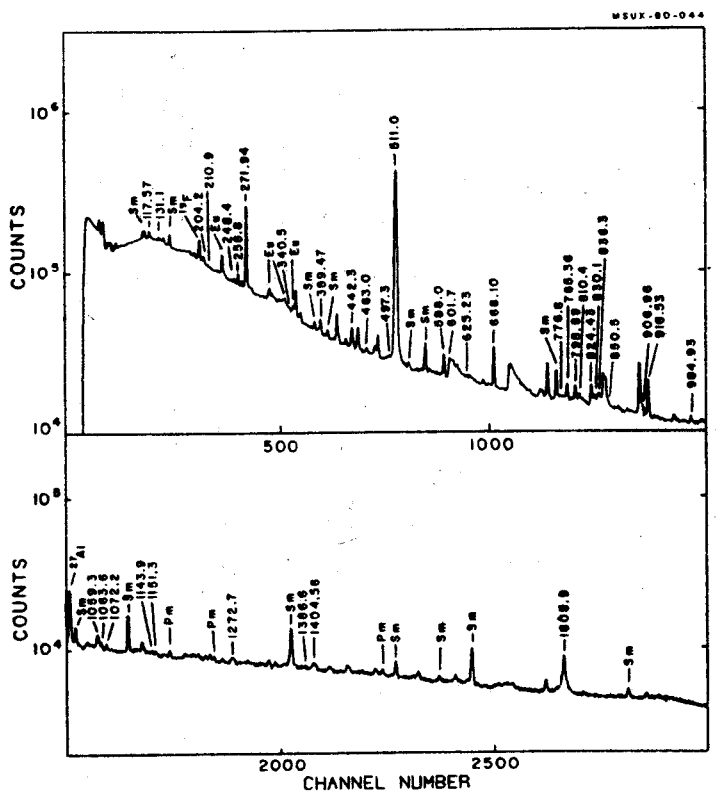

FIG. 1. In-beam singles γ-ray spectrum from the reaction, ^{144}Sm(p,2nγ)^{143}Eu, taken with a 10%-efficient Ge(Li) detector placed at 125°.

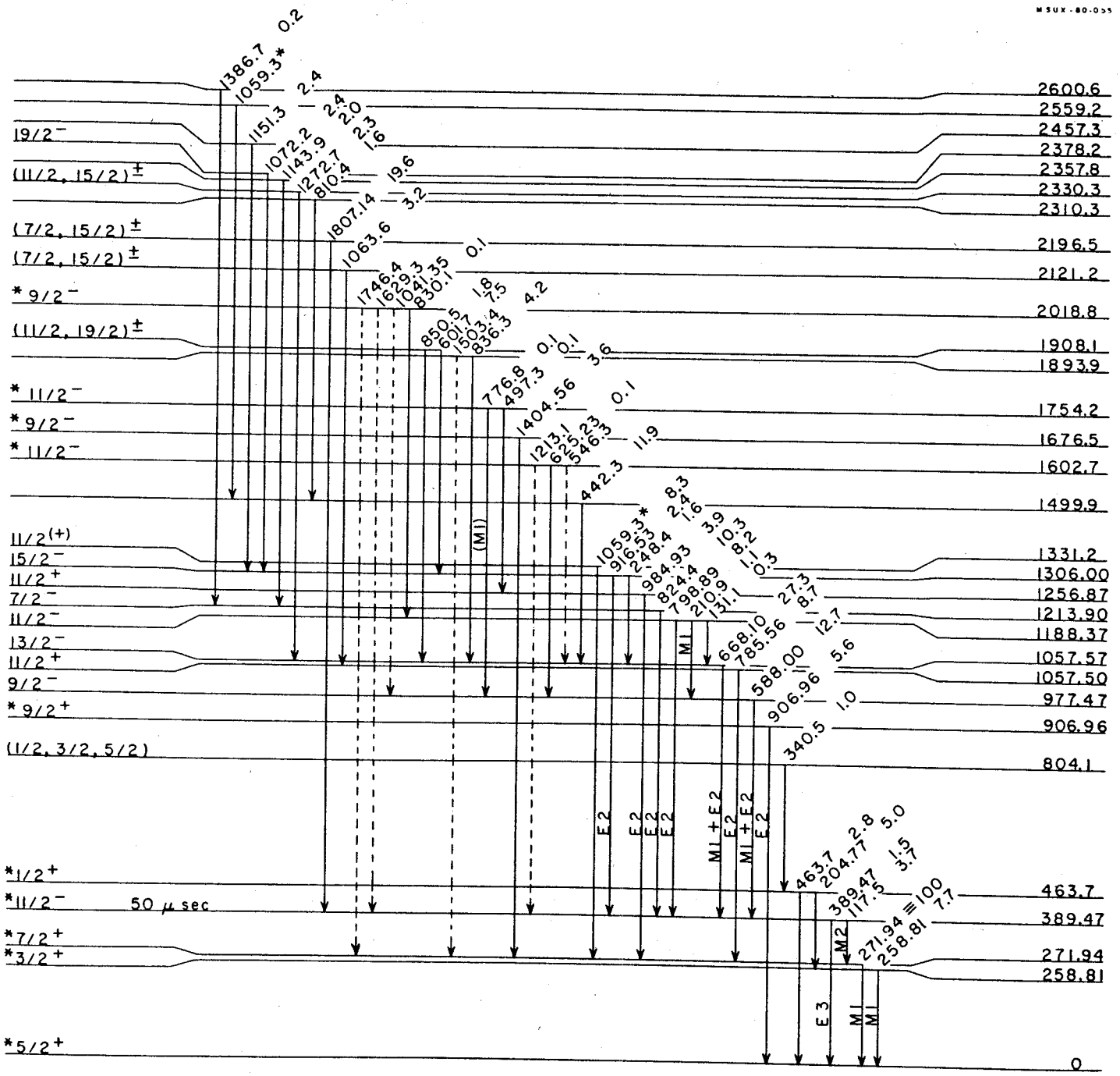

$^{143}_{63}Eu_{80}$

FIG. 4. ^{143}Eu level scheme as determined from the ^{144}Sm(p,2nγ)^{143}Eu reaction.

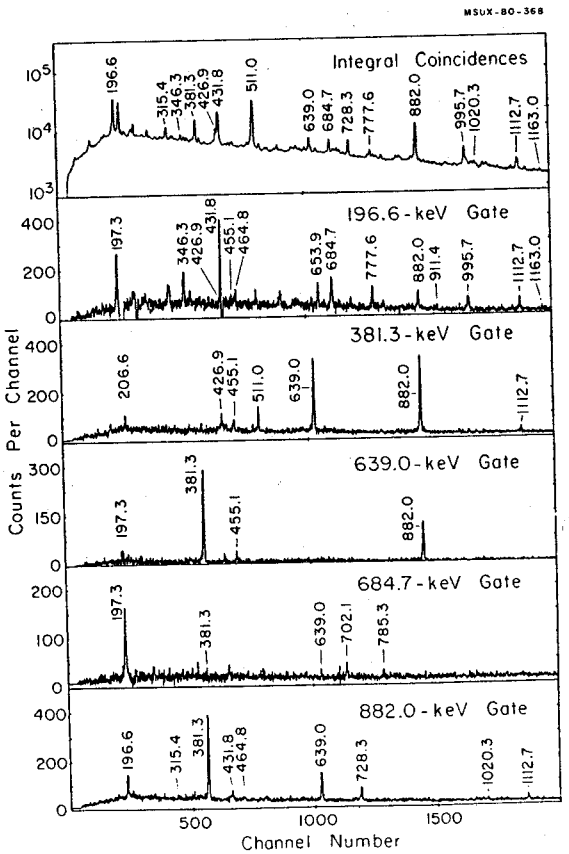

FIG. 2. In-beam γ-γ coincidence spectra from the reaction, $^{141}Pr(\alpha,4n\gamma)^{141}Pm$. The integral coincidence spectrum is shown at the top, with five representative gated spectra below it.

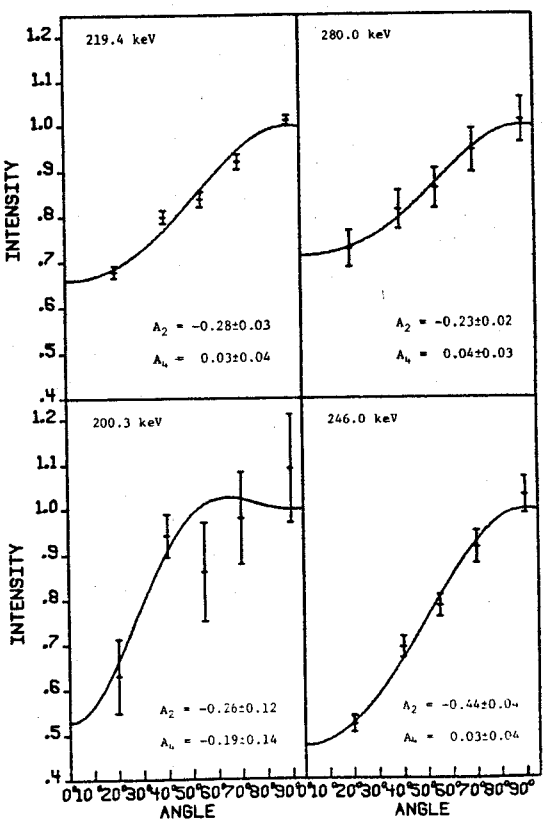

FIG. 3. Four representative angular distributions from the $^{139}La(\alpha,4n\gamma)^{139}Pr$ reaction.

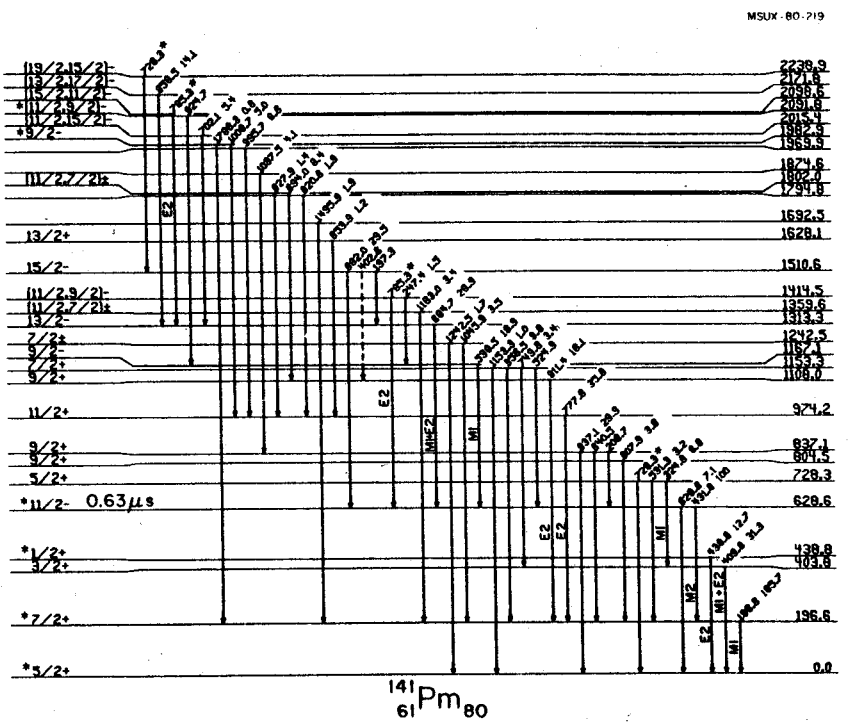

FIG. 5. ^{141}Pm level scheme as determined from the $^{142}Nd(p,2n\gamma)^{141}Pm$ reaction.

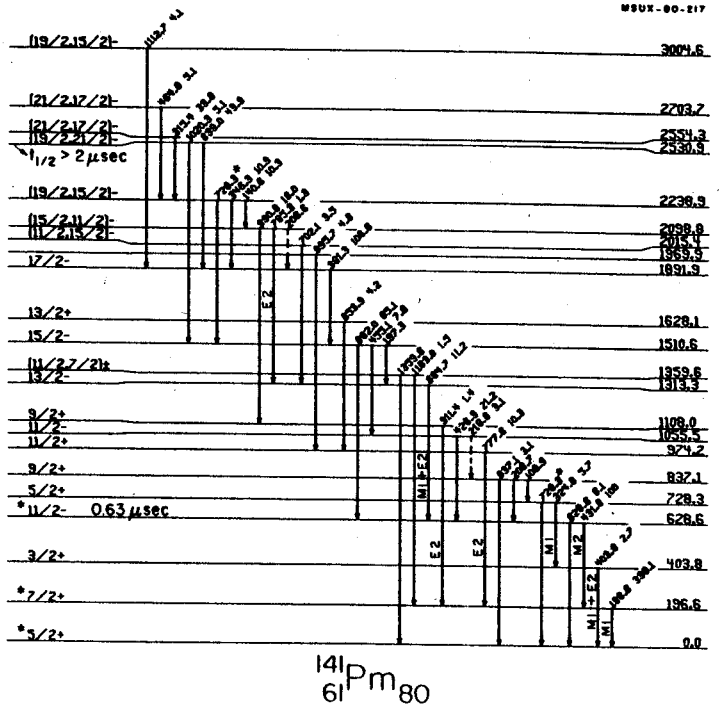

FIG. 6. ^{141}Pm level scheme as determined from the ^{141}Pr(α4nγ)^{141}Pm reaction.

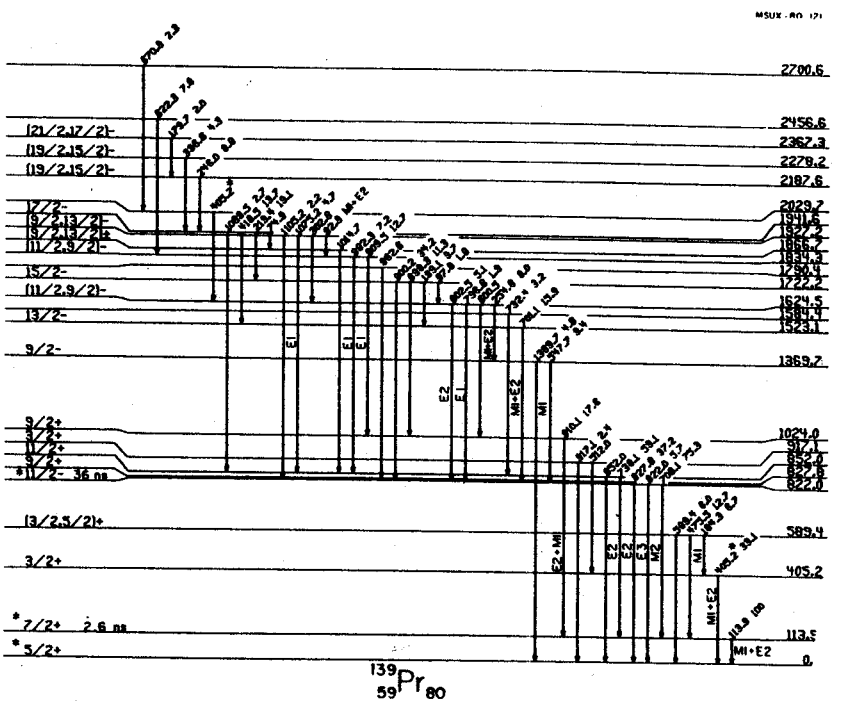

FIG. 7. ^{139}Pr level scheme as determined from the ^{140}Ce(p,2nγ)^{139}Pr reaction.

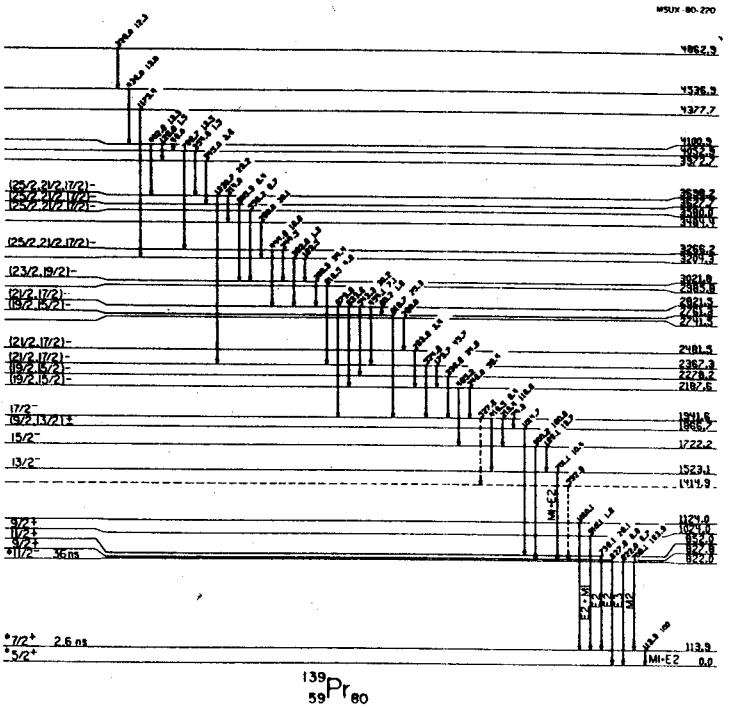

FIG. 8. ^{139}Pr level scheme as determined from the ^{139}La(α,4nγ)^{139}Pr reaction.

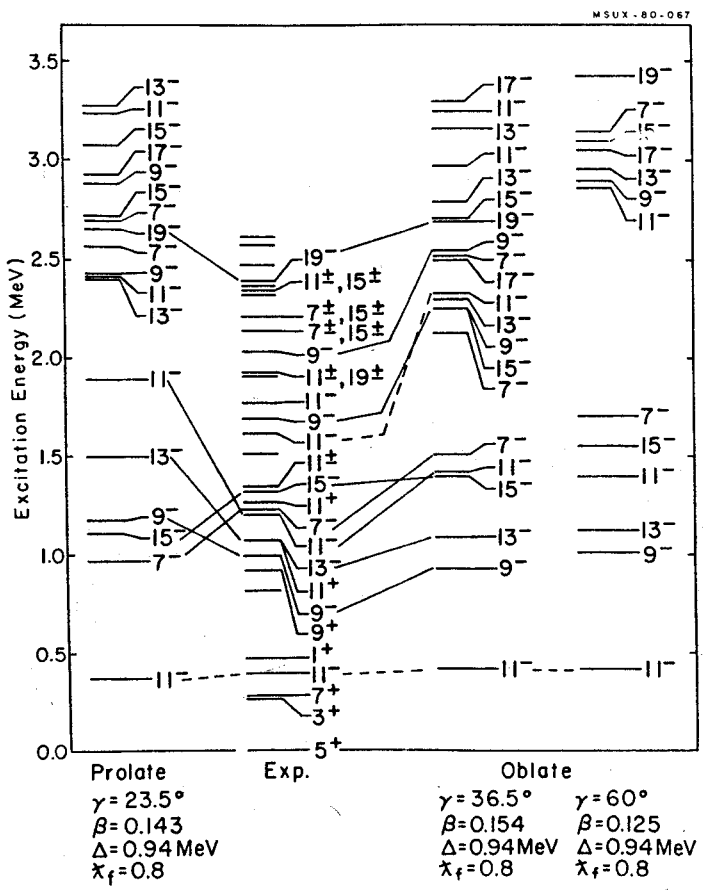

FIG. 9. Energies of calculated negative-parity states in ^{143}Eu compared with our experimental findings. We calculated these energies using a triaxial weak-coupling model, coupling the $\pi h_{11/2}$ state to a deformed core. Results for both prolate and oblate and two different oblate deformations are shown; a slight oblate deformation seems indicated.

The resulting level schemes for the three nuclei are shown in Figs. 4-8. Because the (p,2nγ) and (α,4nγ) reactions excited different sets of states, having remarkably little overlap, we show separate level schemes for ^{141}Pm and ^{139}Pr as excited by each reaction.

We performed triaxial weak-coupling calculations for the states in ^{143}Eu, using the model developed by Meyer-ter-Vehn.[5] Agreement was quite good for the negative-parity states, indicating a slight oblate deformation, but agreement was not so good for the positive-parity states (presumably because of the ease of mixing among the many positive-parity states). The results for the negative-parity states are shown in Fig. 9. We are now embarking on an attempt to the states in all three nuclei in terms of the interacting fermion-boson model.[6] A summary of our overall findings, including comparisons with β decay and (p,t) data, is shown in Fig. 10.

1. R. Aryaeinejad, Michigan State University, Ph.D. Thesis, 1980, report MSUNC-210.
2. ^{143}Eu, R. Aryaeinejad, R.B. Firestone, W.H. Bentley, and Wm. C. McHarris, accepted for publication in Phys. Rev. C (1980).
3. ^{141}Pm, R. Aryaeinejad, W.H. Bentley, P.M. Walker, and Wm. C. McHarris, submitted to Phys. Rev. C (1980).
4. ^{139}Pr, R. Aryaeinejad, W.H. Bentley, and Wm. C. McHarris, submitted to Phys. Rev. C. (1980).
5. J. Meyer-ter-Vehn, Nucl. Phys. A249, 111 (1975).
6. F. Iachello and O. Scholten, Phys. Rev. Lett. 43, 679 (1979).

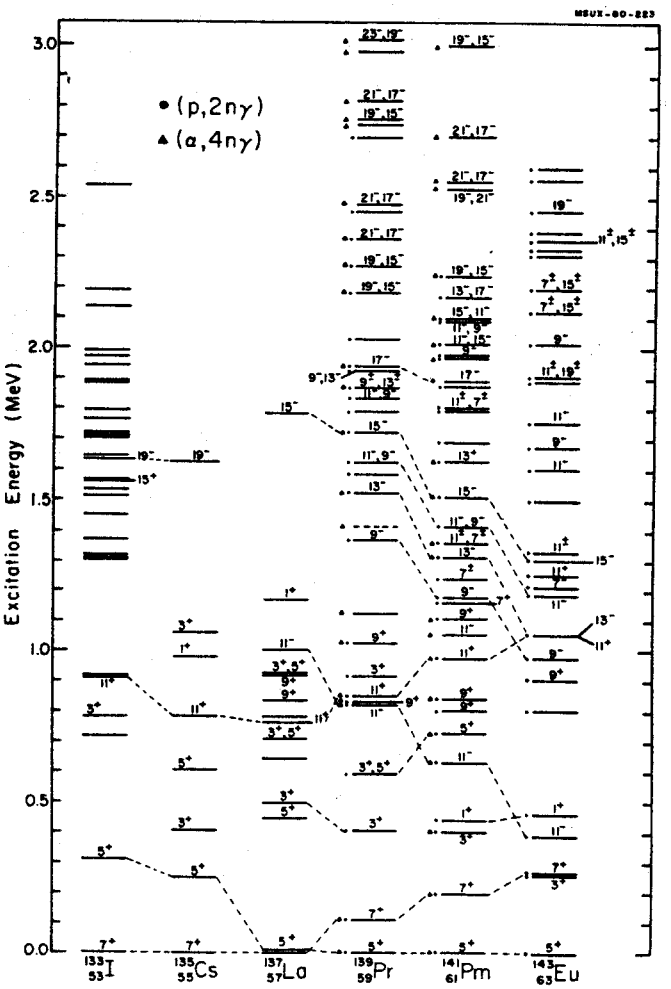

FIG. 10. The positons of known states in odd-mass N=80 isotones, a general summary. (Spins are given as 2J.)

Study on the Structure of Sidebands in ^{168}Yb*

J.L.S. Carvalho, P.M. Walker,+ W.H. Bentley and S.R. Faber++

In the region A=160-180, where many prolate nuclei are found, much work has been done on rotational ground state bands (gsb) up to very high spins. With higher spins the backbending anomaly is observed in almost all rare-earths yet it has not been observed in the even-even N=98 isotones. Another interesting behavior is the low-lying negative-parity bands that seemed to be based on either aligned two quasi-particle configurations (in the region A≃160) or single-phonon octupole vibrations (in the region A≃180).

In order to understand these phenomena the N=98 isotone, ^{168}Yb, is being studied. The experiments performed included γ-γ-t coincidence and γ-angular distribution and they have been described elsewhere.[1] From the coincidence experiment we were able to identify and extend several sidebands in ^{168}Yb that were previously seen.[2] Of particular interest is the identification of a rotational band based on the known I, $K^{\pi} = 5, 5^-$ isomeric level at 1999 keV. We have assigned band members up to 11^- level, by both stretched E2 cross-over and M1/E2 cascade transitions between the levels. Preliminary results from the angular distribution imply the dominance of a two quasi-neutron structure for the band, probably with the $\{5/2^+[642]_n, 5/2^-[523]_n\}_{5^-}$ assignment. The $5/2^+[642]$ neutron comes from the $i_{13/2}$ orbital, and the strong Coriolis effects on the high j=13/2 for this particle can account for the high moment of inertia of the band ($2J/h^2$ 110 MeV^{-1}).

---

* National Science Foundation Grant No. Phy 78-01684.

+ Permanent address: Daresbury Laboratory, Daresbury, Warrington, England.

++ Present address: Argonne National Laboratory, Argonne, Illinois.

1. J.L.S. Carvalho et al., MSU Cyclotron Laboratory Annual Report 1978-1979, p. 42.

2. A. Charvet et al., Nucl. Phys. A197 (1972) 490.